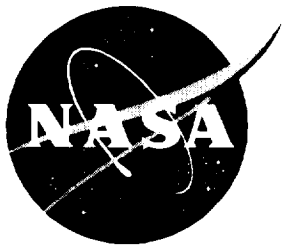

NASA Contractor Report 4632

Investigation of the Effects of Long Duration Space Exposure on Active Optical System Components

M. D. Blue
Georgia Institute of Technology
Georgia Tech Research Institute • Atlanta, Georgia

National Aeronautics and Space Administration
Langley Research Center • Hampton, Virginia 23681-0001

Prepared for Langley Research Center
under Contract NAS1-14654

October 1994

FINAL REPORT

INVESTIGATION OF THE EFFECTS OF LONG DURATION SPACE EXPOSURE ON ACTIVE OPTICAL SYSTEM COMPONENTS

FOREWORD

This report is the final report for NASA Contract NAS1-14654. This contract has had twelve amendments/modifications since the contract began in October, 1976. The amendments extended the contract termination date into 1994, making it the longest running contract at the Georgia Tech Research Institute.

This contract was one of the first set of contracts awarded by NASA to develop experiments to fly on the Long Duration Exposure Facility (LDEF) Satellite. The title of the GTRI program is Active Optical Systems Component Experiment. In this experiment, a varied set of electro-optic components, of the type used in space-based systems, was exposed to the effects of the low-earth orbit environment in order to stimulate any space-induced degradation effects. After satellite recovery, the components were retested to determine the changes in performance resulting from the space exposure.

During the six year period between launch and recovery, many business changes to the electro-optics industry occurred, and some firms which had contributed to this effort went out of business or merged with other organizations. The level of technology also changed so that some of the components became obsolete. These changes made the task of retesting components more difficult than anticipated originally as the planned retest procedure had to be revised in some cases. However, these problems did not prevent the experiment from attaining its objectives. Considerable knowledge has been obtained regarding unexpected degradation in many of the components, and these findings are included in this report.

Georgia Tech is pleased to have been a part of the LDEF program, and thanks the LDEF Chief Scientist, William H. Kinard, and Experiment Managers James Jones, Lenwood Clark, and John DiBattista for their encouragement. We also thank the many other NASA employees, past and present, who have provided their assistance during the course of the work. NASA has made the LDEF program exciting and worthwhile for the Principal Investigators.

June 22, 1994

FINAL REPORT

INVESTIGATION OF THE EFFECTS OF LONG DURATION SPACE EXPOSURE ON ACTIVE OPTICAL SYSTEM COMPONENTS

TABLE OF CONTENTS

TABLE OF CONTENTS CONTINUED

TABLE OF CONTENTS CONCLUDED

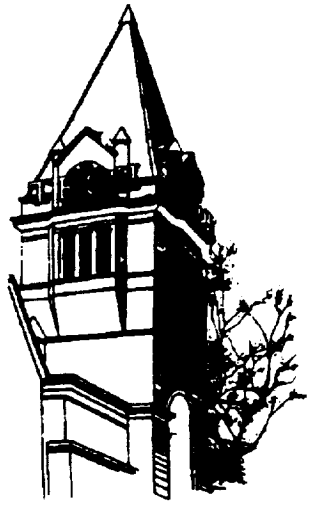

FINAL REPORT

INVESTIGATION OF THE EFFECTS OF LONG DURATION SPACE EXPOSURE ON ACTIVE OPTICAL SYSTEM COMPONENTS

I. INTRODUCTION

1.1 Background

This report summarizes the design, construction, launch preparation, retest, and data analysis of the contents of the Active Optical Components Experiment which was exposed to the effects of low-earth orbit aboard the NASA Long Duration Exposure Facility (LDEF) satellite. In this section, the objectives of the experiment are reviewed. The general design of the experiment and component selection criteria are summarized. A bit of the history of this experiment is also presented for those readers who are unfamiliar with the background of this NASA program which lasted nearly twenty years from start to finish.

Subsequent sections discuss the initial data set and the data taken after retest for the individual components. These results are then reviewed to determine what degraded and why. In the final section, the results from the experiment are summarized in order to provide some guidelines for individual materials and component selection for space-based electro-optical systems.

Our initial work on this program was reviewed by Mr. John DiBattista, experiments manager, and Mr. William H. Kinard, Chief Scientist. As the program progressed, Mr. Lenwood Clark, and later Mr. James Jones, were the experiments managers for the program. The initial proposal and component selection criteria were developed by Mr. Robert Shakelford, Mr. James Gallagher, and Dr. M. D. Blue of the Georgia Tech Research Institute. Many students and faculty members at Georgia Tech contributed to the program as well as many other scientists at industrial and government facilities.

The program was initiated on October 14, 1976 with support from NASA Langley Research Center. With various extensions, the program continued into 1993, a period of over seventeen years.

1.2 Objective

The objective of this experiment was to determine quantitatively the effects of long-duration space exposure on the relevant performance parameters of a representative set of electro-optic system components including lasers, radiation detectors, filters, modulators, windows, and other related components; to evaluate the results and implications of the measurements indicating real or suspected degradation mechanisms; and to establish guidelines, based on these results for the selection and use of components for space-based electro-optic systems.

1.3 Experiment Design

The experiment consisted of placing a selected set of well-characterized electro-optic system components aboard the LDEF, and remeasuring the components after retrieval of the satellite. The major consideration in hardware design was a method of mounting the components to facilitate convenient prelaunch modifications and component changes while meeting the thermal, mechanical, and safety requirements for flight hardware. NASA desired that the experiment be "dry" in the sense that no electrical bias or cooling systems be incorporated in the design.

At the time the experiment was designed, no established degradation mechanisms for such electro-optic components were known to be dependent upon bias potentials or currents. While a limited number of papers indicating the effects of nuclear radiation on the components were found, these effects were not altered by application of normal operating potentials. The radiation levels necessary to cause permanent damage were above the levels expected to be sustained by the LDEF during the planned one year in space. No compelling reasons to include electrical power or bias were found, and the experiment conformed to the NASA request.

As a result, the data gathered by this experiment serve as a baseline for the effects of degradation of the components at ambient temperatures in near-earth orbit. Future experiments can be combined with the ambient-temperature data to separate degradation effects that are specifically temperature related.

Table I. contains a list of the components selected for inclusion in this experiment. Figure 1 shows a sketch of the LDEF and indicates the position of the experiment tray described in this report. The following section describes the mechanical and thermal design of the flight hardware.

Some of the component experiments included in the GTRI tray represented experiments on electro-optical components designed by other groups which were included on the GTRI tray for convenience. These experiments are the following: [1] A set of laser mirrors was provided by scientists at the Air Force Weapons Laboratory, Albuquerque, New Mexico; [2] All but two of the pyroelectric infrared detectors were provided by Dr. James Robertson of the NASA Langley Research Center; [3] A well characterized set of ULE and quartz glass was provided by John Vallimont and Keith Avey of Eastman Kodak Corporation; [4] The UV-sensitive film, detector, filters, and windows were provided by Dr. Gale Harvey of NASA Langley Research Center; and [5] Holographic crystals were provided by Drs. W. R. Callen and T. K. Gaylord of the School of Electrical Engineering, Georgia Institute Of Technology. A description of these experiments and the results obtained are included in this report where possible.

The program was funded in three phases. The Initial phase was concerned with the task of designing the mounting hardware to meet the requirements of manned space flight, to define and acquire the component set, and to perform all needed prelaunch component characterization. The second phase was concerned with qualification testing and other tasks to prepare the experiment for launch. The third phase was concerned with retesting the components. The following sections provide details of the thermal and mechanical design followed by descriptions of the prelaunch and postrecovery performance of the various electro-optical components.

TABLE 1.

COMPONENTS ABOARD THE ACTIVE OPTICAL SYSTEMS COMPONENT EXPERIMENT

Passive Components	Active Components	Detector
Paints		
3M Black	ADP Modulator	Silicon PIN
IITRI Black	Channeltron Array	Silicon pn Diodes
Cat-A-Lac Black	GaAlAs Laser Diodes	Silicon Gamma-Ray Detector
Chemglaze Z306	Laser Diode Arrays	AlGaAsP PV
Chemglaze Z302	GaAsP LED's	InSb PV
Martin Black	CO_2 Laser	PbS PC
	HeNe Laser	PbSe PC
Neutral-Density Filters	Laser Flashlamp	HgCdTe PV
Narrow-Band Filters		HgCdTe PC
Hot Mirrors		PdSi Arrays
Lyman-Alpha Filters		UV Si
1600 Å Filter		UV PMT
UV Mirror		Pyroelectric
Black Polyethylene		$LiTaO_3$
Optical Glasses		$Sr_{.66}Ba_{.33}Nb_2O_6$
Window Materials		TGS
MgF_2		UV Photomultiplier
Al_2O_3		UV Silicon Detector
CaF_2		
LiF		
SiO_2		
35-mm UV-sensitive Photographic Film		

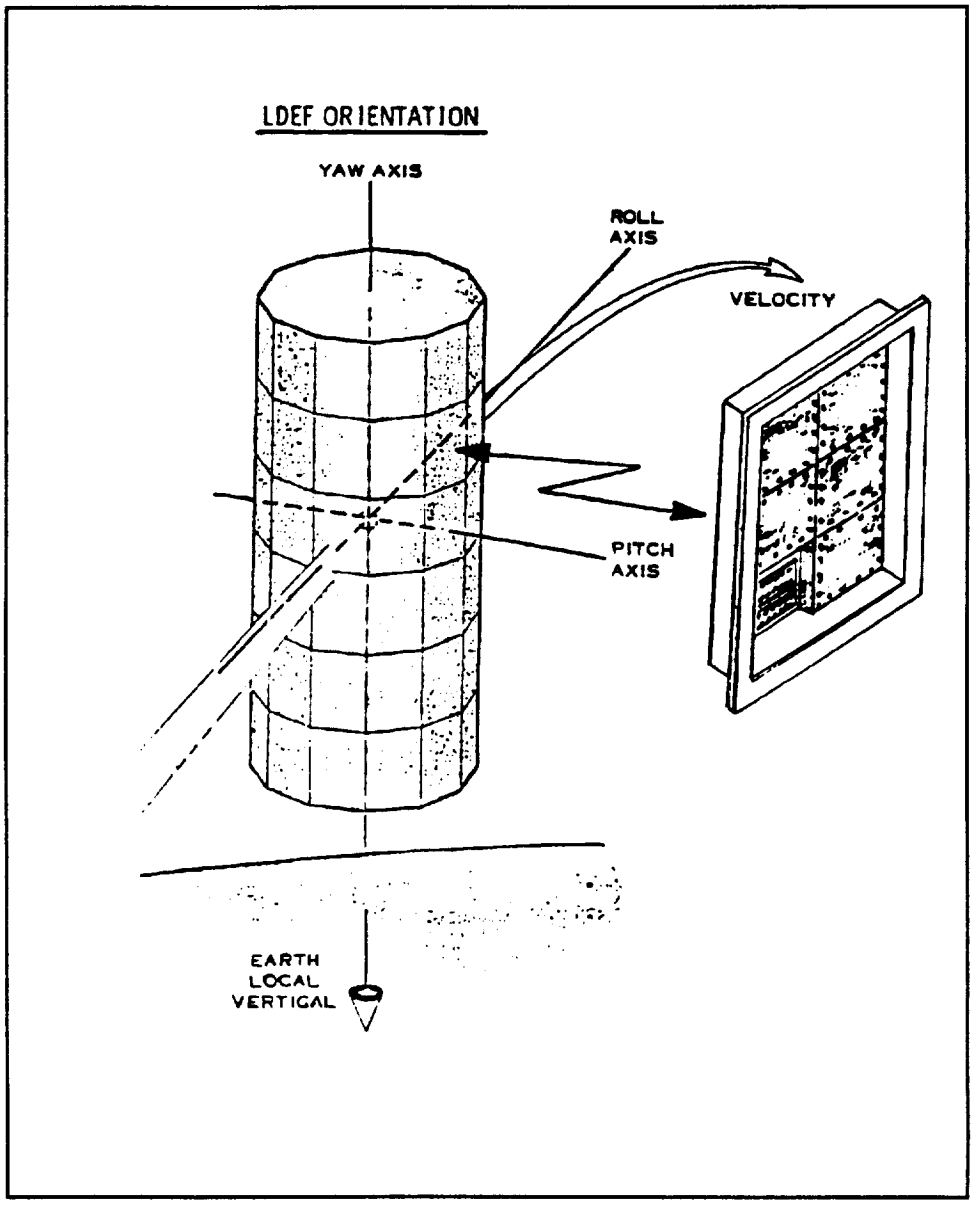

Figure 1. Position Of The GTRI Tray On The LDEF Satellite

II. THERMAL CONSIDERATIONS

2.1 General

Ambient temperature limitations vary substantially among the components included in the LDEF electro-optic component set. A maximum temperature of 85 °C applies to the ADP material used in the light modulator. Above this temperature, upper temperature limits for infrared detectors range from 100 °C for HgCdTe detectors to 145 °C, the softening point of the indium-alloy solder used for lead attachment. Minimum temperatures were not considered to be a problem. Maximum temperatures were maintained through the use of surface coatings of defined emissivity and absorptivity. Sunscreens were used on all but one subtray to minimize the excursions about the maximum design temperature should the LDEF experience unplanned orientations or orbital parameters. Maximum temperatures were not a strong function of the percentage transmission the sunscreens.

2.2 Thermal Control Materials

The LDEF 6-inch regular tray is constructed of 6061-T6 aluminum sheet. The six subtray base plates are also of this material, 1/4-inch in thickness, and bolted to a frame constructed of 6061-T6 aluminum angles. Components are mounted typically on 6061-T6 aluminum sheet 0.06-inch thick which has been formed to a hat-shaped cross-section, and bolted to the LDEF base plates.

All four sides of the tray were assumed to have an anodized coating with values of solar absorptivity/IR emissivity of (α/ε) of (0.30/0.20). The bottom of all tray frames and all experiment surfaces facing the interior of the vehicle were assumed to be painted with Chemglaze Z306 polyurethane black paint with values of solar absorptivity/infrared emissivity (α/ε) of (0.92/0.90). The bottoms of the main structural intercostals facing the vehicle interior were also assumed to be coated with this paint.

2.3 Thermal Environment

The general thermal environment used for thermal analysis of the LDEF tray is presented in Table 2. Energy sources include incident direct solar energy, solar energy reflected from the earth assuming an earth reflectance of 1.0 (variable), and incident infrared energy emitted by the earth. The numbers for reflected solar energy when multiplied by the appropriate albedo (earth reflectance) factor, give the actual values of incident reflected solar energy. Albedo factors vary from 0.3 to 0.4.

2.4 Radiation Analysis Method

The basic method used to analyze the thermal control techniques for the LDEF tray was the manipulation of surface coating properties to produce the desired temperature values. Thus, it is important to accurately model the radiation heat transfer to and from the tray and its contents.

TABLE 2.

BOUNDARY TEMPERATURES AND FLUX DATA
FOR LDEF SAMPLE TRAY ANALYSIS

EXTERNAL SURFACE FLUX DATA

Cold Case Environmental Flux Data: Regular Tray

Solar Energy =	0.0 BTU/HR-FT^2
Reflected Energy =	0.01 BTU/HR-FT^2
Earth Energy =	22.11 BTU/HR-FT^2

Hot Case Environmental Flux Data: Regular Tray

Solar Energy =	470.73 BTU/HR-FT^2
Reflected Energy =	8.20 BTU/HR-FT^2
Earth Energy =	12.57 BTU/HR-FT^2

BOUNDARY TEMPERATURES (°F)

Description	Hot Case	Cold Case
Average Vehicle Interior	+130	+10
Structure Hot Side	+160	+40
Structure Cold Side	+100	-5
Space (Sink)	-460	-460

Several different cases were considered. Analysis showed that heat conduction between the base plate and the hot sections upon which the components were mounted played a predominant role in the heat transfer mechanism. During subsequent modeling, the hat section and the plate were assumed to have the same temperature.

Figure 2. shows the results for the case selected for our implementation of the LDEF tray. A sunscreen is used over the base plate and hat sections. It is assumed to have an anodized coating with values of (α/ε) of (0.30/0.13). For different fractions of screen opening, f_s, the hot and cold temperatures of screen and hat sections are graphically represented. The screens used

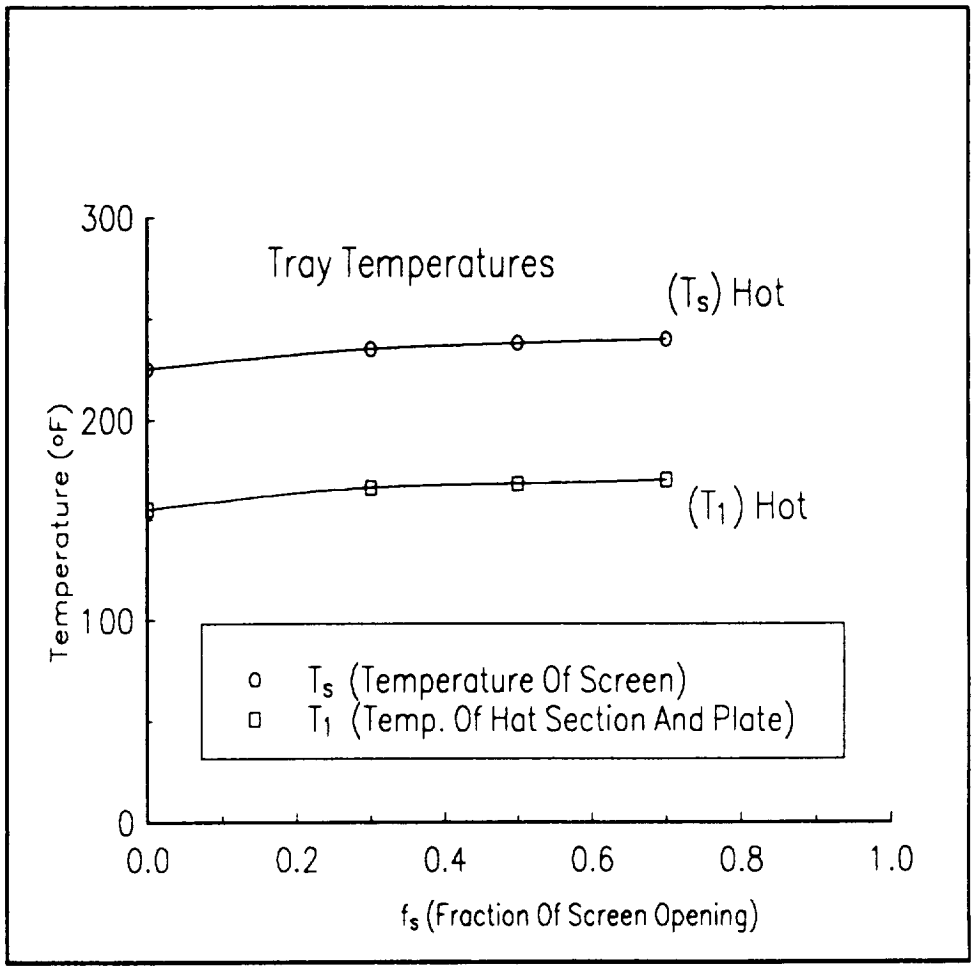

Figure 2. Calculated variation of the maximum and minimum tray temperatures as a function of sunscreen opening.

on the LDEF tray had a value for f_s of about 0.45 over the central region, but a value of 0.36 for the screen as a whole because of a border without holes for attachment to aluminum channels at the edge of the base plates. The resulting analysis indicated an upper limit (or maximum) temperature near 180 °F or 82 °C for the case implemented. Actual temperatures will not reach the extremes shown in Figure 2. because of the thermal inertia of the system as it cycles between the maximum and minimum limiting cases. Therefore, the desired temperature control was attainable in principal with proper coatings and thermal design. Temperature data from the LDEF (Section IV) indicated that the thermal analysis for the tray was quite satisfactory.

Figure 3 shows the general construction of one of the six subtray panels which resulted from thermal analysis and mechanical design considerations. To avoid possible complications is determining total flux on samples, one subtray did not use a sunscreen. Mechanical design considerations are discussed in the following section.

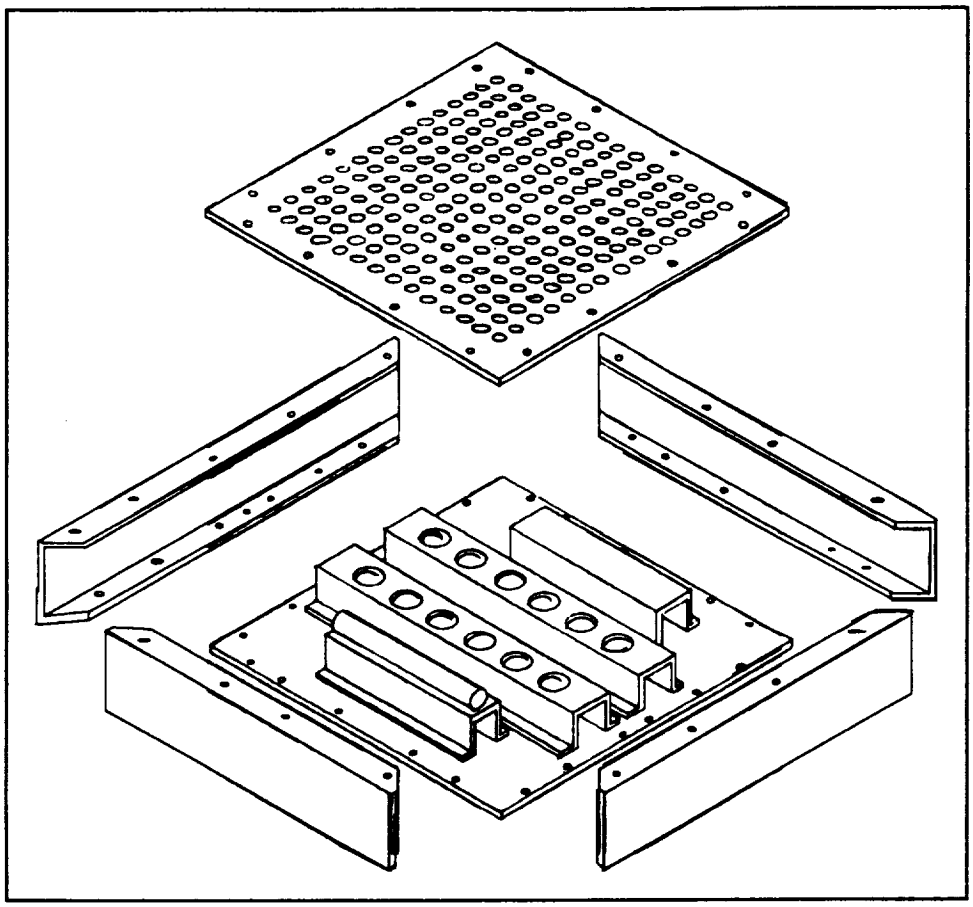

Figure 3. Typical subtray panel construction.

III. STRUCTURAL DESIGN

3.1 Resonance And Stress Effects

The 16.25" x 16" tray subpanel was made from 1/4" aluminum plate. The resonant frequency of the bare plate was estimated to be 173 Hz. The addition of the hat-shaped sections for mounting components increases the rigidity of the plate, and raises the natural frequency. The sunscreens were expected to have a lower vibrational frequency, less than 100 Hz.

During vibration tests using one subpanel (one of six), the only resonant frequency with appreciable amplitude occurred at 94 Hz. This resonance was caused by the sunscreen vibrating in a direction normal to the tray surface. This resonant frequency occurs outside the critical range for both the Qualification and Flight Assurance requirements. Other weak resonant vibrations were observed at 270 and 330 Hz, and were not large enough to be of concern. The Qualification Test required a level of 0.225 g^2/Hz (10.97 g rms) for a duration of 60 seconds.

Vibrational analysis and testing of this subpanel indicated that the design produced no unusual or unexpected vibrational resonances, and all vibrational amplitudes were within LDEF test specifications.

Calculated stress levels on the structure were near 50 psi; a safe value. Weight of the experiment was not a major consideration, and therefore considerable design freedom was possible. The final experiment weight was 125.08 pounds, with an unbalance of 5.4 foot-pounds. Maximum allowed weight for the tray was 175 pounds.

3.2 Hardware Design

Thermal expansion of the screen relative to the support structure could be accommodated by making the holes for the mounting screws 0.032 inches larger than the screw diameter. The sun screen was sandwiched between two 1/8 inch thick silicon rubber gaskets. The compressibility of the silicon rubber allowed the sunscreen to expand or contract without direct metal-to-metal contact at the mounting surfaces, thus preventing structural stresses on the subtray panel itself.

Materials for the construction of the experiment hardware are listed in Table 3.

TABLE 3. MATERIALS FOR SUPPORT FIXTURES

Major Materials Used In The GTRI LDEF Experiment
Are The Following

Aluminum:	Sheet, bar, rod	6061-T6
	sun-shield support channel	6062-T52
Fiberglass:	Epoxy fiberglass G-10 grade Mil-P-139490	
Gaskets:	Silicon rubber	Chorlastic R-500
Fasteners:	Floating inserts and machine screws 304 and 304 stainless steel	
Paint:	Black paint	Chemglaze Z-306 Flat Black
Anodize:	Chrome anodize with α/ε = 0.3/0.2	

All materials conformed to NASA requirements. All fixtures for the tray were cleaned with detergent, rinsed with distilled water, and wiped with methyl alcohol before assembly. The fixtures and electro-optic components were stored in a clean room at constant temperature before final assembly and shipment to NASA.

When the LDEF was retrieved and returned to Kennedy Space Center, the tray was found to be in excellent condition. There were no damaged components, no evidence of poor cleaning, and no visible fingerprints (a tribute to our student workers). The effects of space exposure could be seen in the surfaces stained with contaminant believed to be residue from the Z306 black thermal control paint and other outgassed vapors from the LDEF structure and payload.

Additional details regarding this contaminant film are discussed in Section VIII.

The green epoxy-fiberglass strips used to mount most electro-optic components on the GTRI tray had changed color to a walnut brown where their surfaces had been directly exposed to the space environment. Where the green surfaces were protected or covered, they retained their original color. The overall mechanical/thermal design and the experiment preparation procedures were successful.

IV. THE LDEF ENVIRONMENT

4.1 General

The LDEF was launched was launched into orbit by the Space Shuttle Challenger mission 41C on April 6, 1984. The satellite was deployed on April 8, 1984. The original altitude of the circular orbit was 258.5 nautical miles (479 km) with an orbital inclination of 28.5 deg. The LDEF remained in orbit far beyond its initially planned six to twelve month mission.

At retrieval it had been orbiting for five years and nine months and had completed 32,422 orbits. It was retrieved by the Space Shuttle Columbia on January 11, 1990. At recovery, the LDEF altitude had decayed to 175 nautical miles (324 km). At a lower altitude, near 150 nautical miles, the satellite would begin to tumble and could no longer be recovered. At the rate of descent in January, 1990, the time available to recover the LDEF was about six weeks.

4.2 Tray Environment

The GTRI tray was mounted in position E5 which means that it was one row down from the top row of trays and was in the four o'clock position (or facet) where twelve o'clock represented the leading edge facet. Figure 1 shows the orientation. Thus, the GTRI tray was on the trailing side of the structure. The trailing side trays experienced a lower fluence of atomic oxygen and fewer micrometeoroid hits than the leading-edge trays.

The major environmental parameters relevant to the components on the GTRI tray are summarized in Table 4.

TABLE 4.

ENVIRONMENTAL PARAMETERS DETERMINED FOR THE LDEF E5 POSITION

Maximum Temperature:	66 °C
Minimum Temperature:	-10 °C
Atomic Oxygen Fluence:	3.7×10^{12} atoms/cm^2
Equivalent Solar Hours:	8200 Hrs.

Radiation Dose (Electrons and Protons)

Surface Dose:	300 krad (approx.)
Under Flat Packs:	600 rads (approx.)
1/16-thick Al cover:	300 rads (approx.)

These radiation dose values are conservative. The sun screens covering most subtrays will reduce these values by about 50% depending upon LDEF orientation.

Maximum and minimum tray temperatures varied with position. From NASA documents[1], the important environmental variables at the GTRI tray position (E5) can be determined. The total radiation dose for unshielded samples was less than 300 krads(Si), mainly caused by geomagnetically trapped electrons with a small amount of proton irradiation.[2] The electron fluence for unshielded samples for all electron energies was less than 2.5 X 10^{12} electrons/cm^2. Samples mounted under an aluminum cover received less than 300 rads(Si). Devices mounted in flat packs which were inverted would have received less than 600 rads(Si). These irradiations are not large, but can produce observable effects in the most sensitive components (i.e. CCD devices).

The total fluence of atomic oxygen was determined to be 3.7×10^{12} for the E5 tray position[2]. This is approximately one oxygen atom for each 100 surface atoms, and should not produce significant effects.

Maximum temperatures in space at the E5 tray position were believed[3] to be about 66 °C and minimum temperatures were believed to be near -10 °C. These temperatures were within the design limits. Minimum temperatures were not of concern. Maximum temperatures were of concern.

V. OPTICAL FILTERS AND MIRRORS

5.1 Optical Substrates And Coatings

Twelve optical substrates and coatings were carried on the tray for an Eastman Kodak Company experiment. This experiment contained three fused silica substrates, three ultra-low expansion (ULE) uncoated glass samples, two ULE samples with a high-reflectance silver coating, two fused silica with an antireflectance coating (SiO_2/TiO_2 layer pair), and two fused silica samples with a solar-rejection coating.[4] Duplicate samples were stored by Kodak for comparison purposes. All samples were 1.25 inches in diameter by 0.25 inches in thickness with all faces and edges polished. These samples were not covered by a sunshield, and received full exposure to the space environment.

After retrieval, the samples showed one micrometeroid impact site and all were coated with the typical light-brown stain which could be removed (from all but one antireflection coated sample) using isopropyl alcohol. As for the stain on the antireflection-coated sample, neither acids nor organics would remove it. Three hours exposure to an oxygen plasma reduced the brown coloration and increased the transmission.

Analysis showed that the brown coating contained carbon as a 30-Å surface layer in addition to a layer of polymer containing Si (in the form of silicones and SiO_2). This polymer layer may have fused into the upper surface of the antireflection coating in at least one case.

Although the ionizing radiation fluence was near $3x10^5$ rads(Si), no darkening of the ULE or the fused silica was found. After cleaning the samples, optical transmission agreed with prelaunch measurements.

Optical transmission was measured from 350 to 1200 nm. The brown stain reduced transmission mainly in the short-wave spectral region. The exact spectral characteristics depend upon the density of the stain. Figure 4 shows transmission for one of the uncoated ULE samples where the heaviest deposits were found. This experiment and the UV components experiment indicated that the density of deposited stain material varied with the character of the substrate, presumably indicating a variation of the sticking coefficient for the arriving detritus.

Bidirectional reflectance measurements were made by Kodak on the high-reflectance silver-coated sample (with its contamination layer) and compared to the stored sample. At angles a few degrees off normal, postretrieval measurements indicated that the flight sample had increased light scatter by a factor of ten over the stored sample.

Stress measurements on the samples indicated that the deposited brown coating induced a compressive stress in the uncoated glass and high-reflectance silver coated samples, and no measurable stress in the fused silica antireflectance coated samples. No significant change was found for the control samples. The samples with the solar-rejection coating could not be measured for stress.

These results have recently been reported.[4] For further details, the reader should contact Keith Havey, Arthur Mustico, or John Vallimont of Eastman Kodak Company. Their cooperation in this overall program is sincerely appreciated.

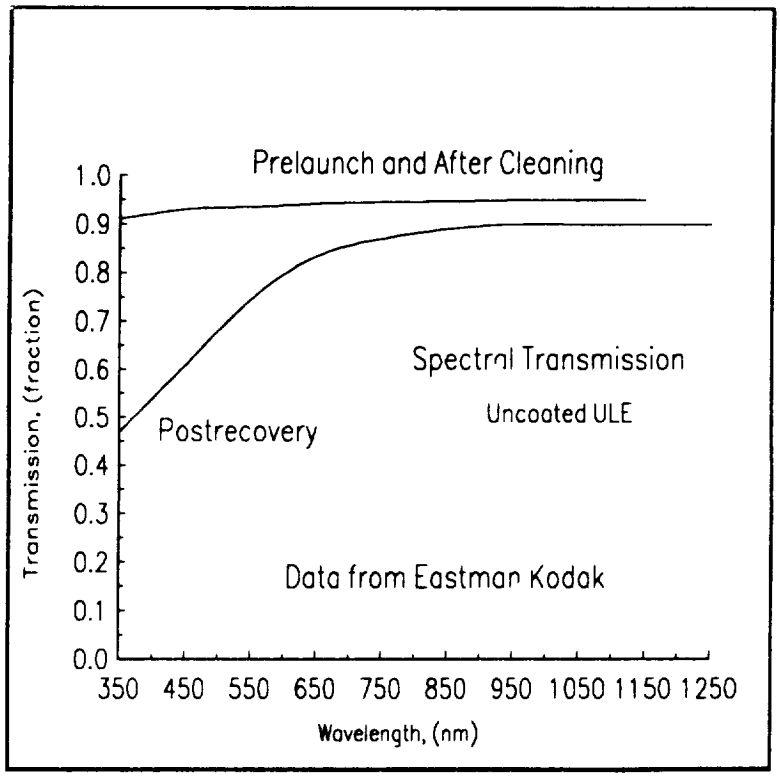

Figure 4. Ultraviolet transmittance for an uncoated ULE-glass sample showing transmittance loss due to a contamination layer (Kodak data).

5.2 Ultraviolet Optical Components

Dr. Gale A. Harvey of NASA Langley Research Center has prepared reports discussing the characterization of the 15 windows, UV filters, and other components which he provided for the GTRI tray.[5] In general, all components were retrieved in good condition. The main spectral interval of interest was 100 to 300 nm. Surface contamination was the only deterioration that was noted. A faint brown stain was found on the front surface of the window materials, and three of the fluoride windows had a brittle film on the back surface. The absence of a film on the back surface of the SiO_2 window (as determined by the absence of IR absorption at 3.4 μm) indicates that the contaminate film depositions were dependent on the substrate material. As the discussion on the following pages indicates, the organic film on the multilayer dielectric filters for the optical region did not produce measurable absorption in the visible spectral region. However, as Fig. 5 from Harvey's work indicates, substantial absorption can be found at shorter wavelengths.

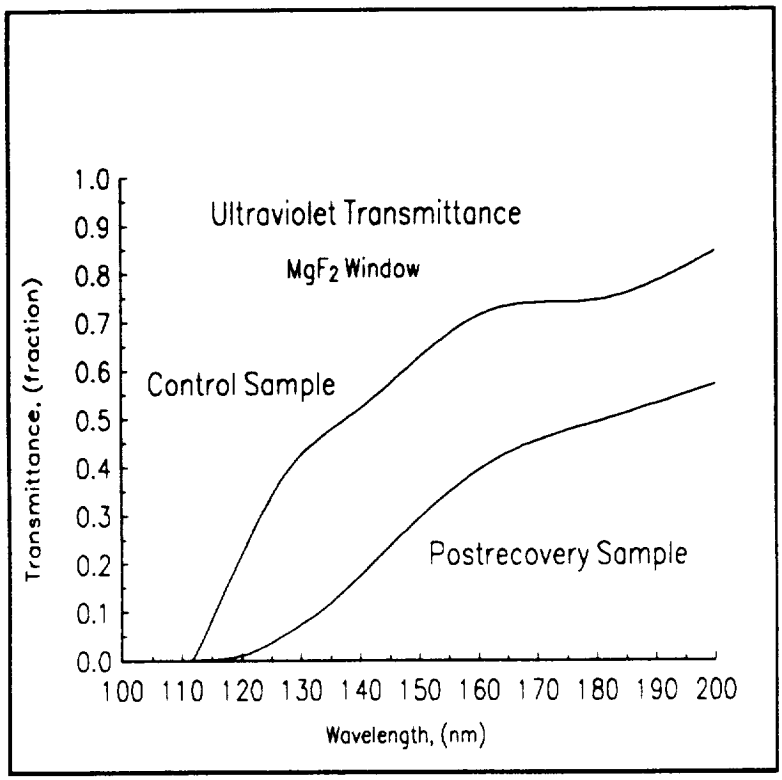

Figure 5. Ultraviolet transmission of a MgF_2 window with front-surface contamination after recovery. Other windows were more strongly affected in this spectral region (Reference 5).

5.3 Visible Region Optical Filters

The set of nine optical filters included three different types,[6] as listed in Table 5. Three of the nine filters were under an aluminum cover (numbers 2, 6, and 9), while the remainder were exposed directly to the space environment.[7]

The filters were fabricated using technology appropriate to the late 1970's. One of the wide-band hot-mirror filters was examined using SEM and SIMS as part of the post-recovery measurements. It was found to be composed of eleven layers of (Thorium Fluoride/Zinc Sulfide) pairs deposited on a glass substrate. The topmost layer was Thorium Fluoride.

Thin-film dielectric-stack narrow-band interference filters used in the experiment reported here were manufactured by cementing two filter halves together so as to protect the interference layers at the center of the sandwich. Neutral density filters had an inconel coating providing an optical density of about 1.4. As mentioned previously, the hot-mirror interference filters were deposited on glass with a ThF_4 layer at the surface.

TABLE 5.
OPTICAL FILTER PROPERTIES

NARROW-BAND FILTERS

Filter No.		Center Wavelength		Band Width		Percent Transmission	
		Before	After	Before	After	Before	After
		nm				Percent	
1		486.2	487.2	1.2	1.4	32.3	25.4
2	Covered	513.9	513.8	1.05	1.9	58.3	28.6
3		633.6	632.5	1.0	5.5	45.1	8.3
4		545.8	544.2	10.7	10.7	62.4	33.0
5		544.7	545.3	10.7	10.8	70.1	33.0

NEUTRAL DENSITY BAND FILTERS

	50% On Wavelength		50% Off Wavelength		% Transmission	
	Before nm	After	Before nm	After	Before	After
6 Covered	415	388	700	780	96	78
7	386	385	695	702	98	86

BROAD BAND FILTERS

Percent Transmission at listed wavelength

Wavelength (nm)		350	400	500	600	700
8	Before	3.2	3.5	3.8	4.0	
	After	3.7	4.1	4.2	4.2	
9	Covered Before	3.0	3.2	3.5	3.7	
	After	2.9	3.1	3.3	0.7	3.7

After measurement but before launch, the filters were mounted on the experiment tray which was then placed within a sealed metal shipping container with desiccant to assure a dry atmosphere. A prompt launch and recovery were planned, and no filters were stored on the ground. Various delays and problems with the space shuttle turned a planned six- to ten-month period in orbit into a 5.8-year orbiting period after an unplanned seven years in storage in various locations before launch. As a result, data are limited to a set of pre-launch and post-recovery measurements

The design and fabrication of optical filters has recently been reviewed by Goldstein[8]. Previous measurements on the effects of space exposure for these types of optical filters are limited. Nicoletta and Eubanks[9] studied the effect of electron, proton, and uv irradiation on the transmittance of various fused silicas, colored glass filters, and thin-film interference filters. They found that no significant changes occurred in the transmittance of fused silica as a result of exposure to electron and proton radiation equivalent to 1 year in space. There was also no change in transmittance of interference filters (shielded with fused silica) as a result of exposure to electron radiation equivalent to 1 year in space. For higher fluences and greater electron energies, transmittance losses in fused silica were observed. Their estimates of the total dose for one year, based on early NASA data, are close to the recent NASA estimates for the 5.8-year LDEF exposure. Therefore, one would not expect measurable changes in optical transmittance from the radiation dose received by the LDEF. Nicoletta and Eubanks did find that exposure to electron fluences of $2x10^{14}$ electrons/cm^2 or greater with electron energies of 1.0 MeV and higher caused significant losses in transmittance for fused silica. Such fluences are higher than the fluence received by the LDEF components.

Reduction in transmittance as a result of ultraviolet irradiation was observed by these authors for interference filters, whereas the filters were unaffected by an initial irradiation by electrons. The authors' tentative conclusion regarding the cause of the measured filter degradation was that the thin-film materials and/or the organic-based adhesive used to assemble the filters were responsible.

More recent measurements also indicate radiation-induced darkening in optical glasses and epoxies[10,11,12]. Typically, measurements are made immediately after irradiation so as to minimize spontaneous recovery. For the measurements reported here, the repeated temperature cycling to temperatures close to room temperature while in orbit followed by similar warming during recovery would permit some annealing of radiation-induced defects. For this reason also, no significant effects on the filter properties resulting from ionizing radiation received while aboard the LDEF were expected.

5.3.1 Results

The narrow-band filter transmittance characteristics for our set of five filters are shown in Figures 6-12. Filter 5 shows a slight but measurable shift toward longer wavelengths as a result of space exposure, but with the same bandwidth. For the other narrow-band filters, the shift is toward shorter wavelengths and is more pronounced. The exception is filter number 2 which was under an aluminum cover. For filter number 2, the filter bandwidth was unchanged. For filter number 3, the filter bandwidth increased substantially. For the other two narrow-band filters, the filter bandwidth did not change appreciably with space exposure.

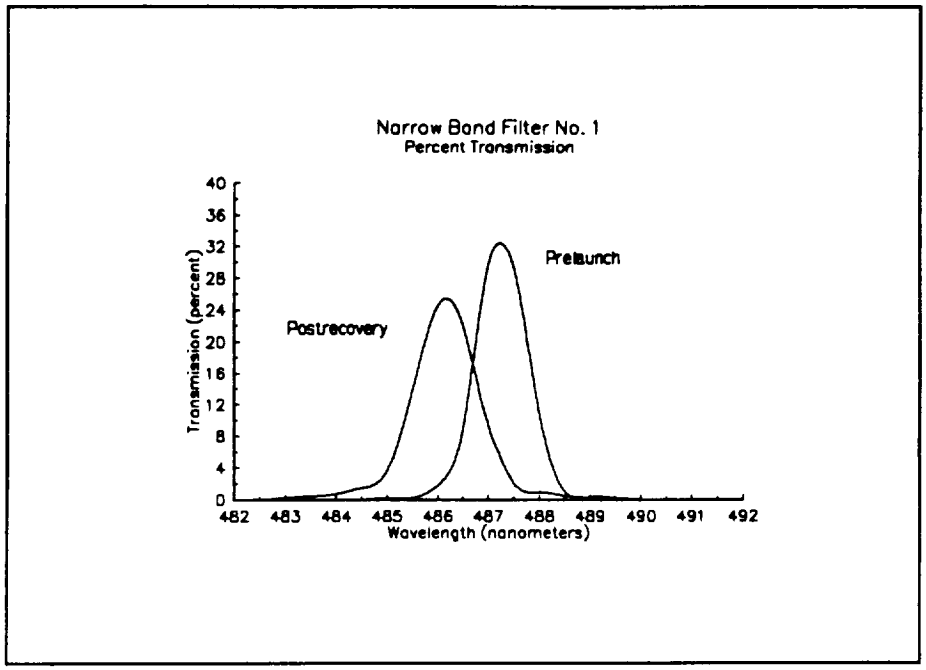

Figure 6. Prelaunch And Postrecovery Transmission Of Narrow-Band Filter Number 1.

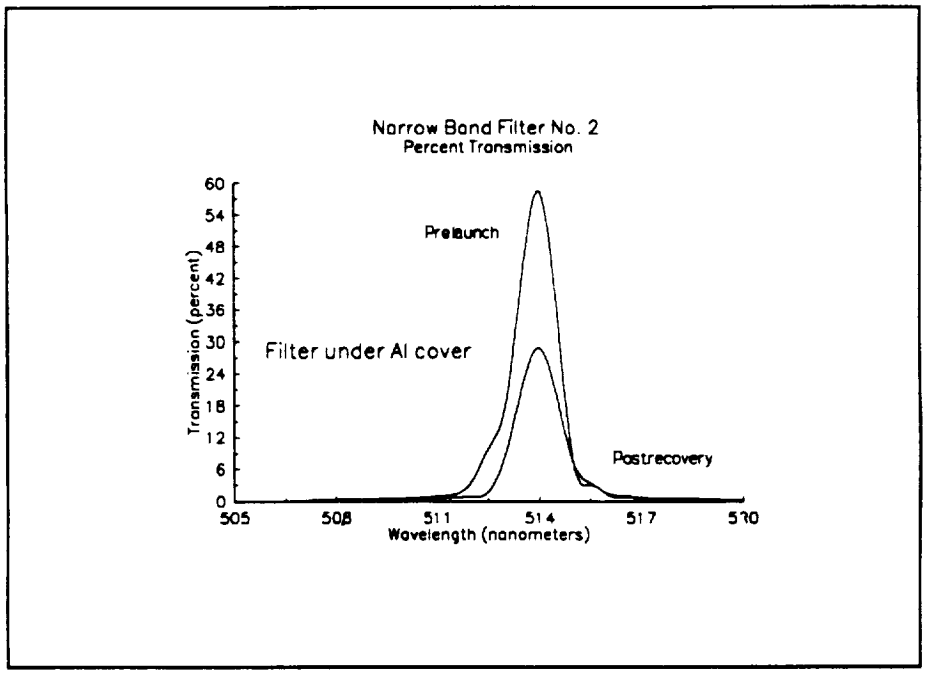

Figure 7. Prelaunch And Postrecovery Transmission Of Narrow-Band Filter Number 2. This Filter Was Protected From The Space Environment By An Aluminum Cover.

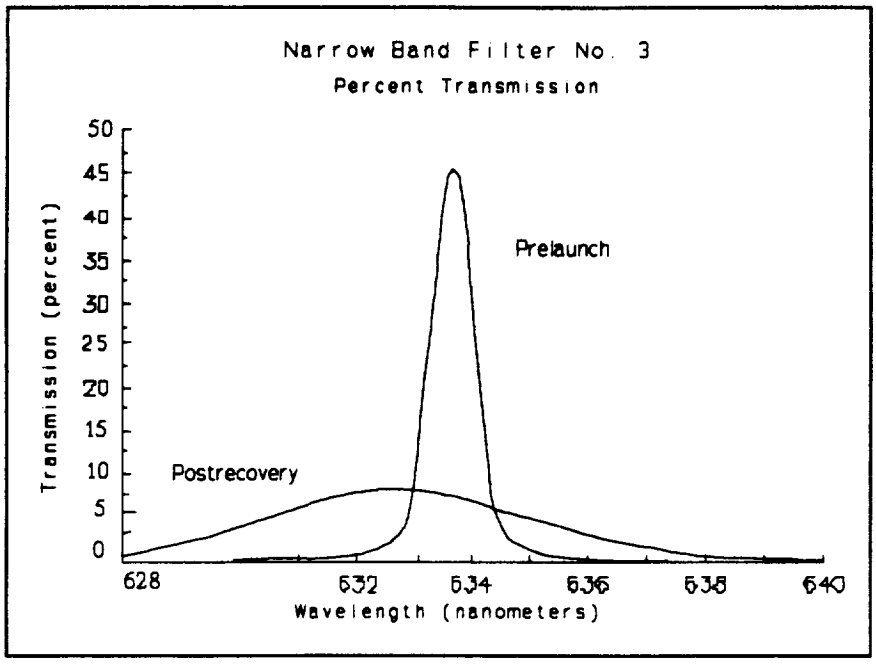

Figure 8. Prelaunch And Postrecovery Transmission Of Narrow-Band Filter Number 3.

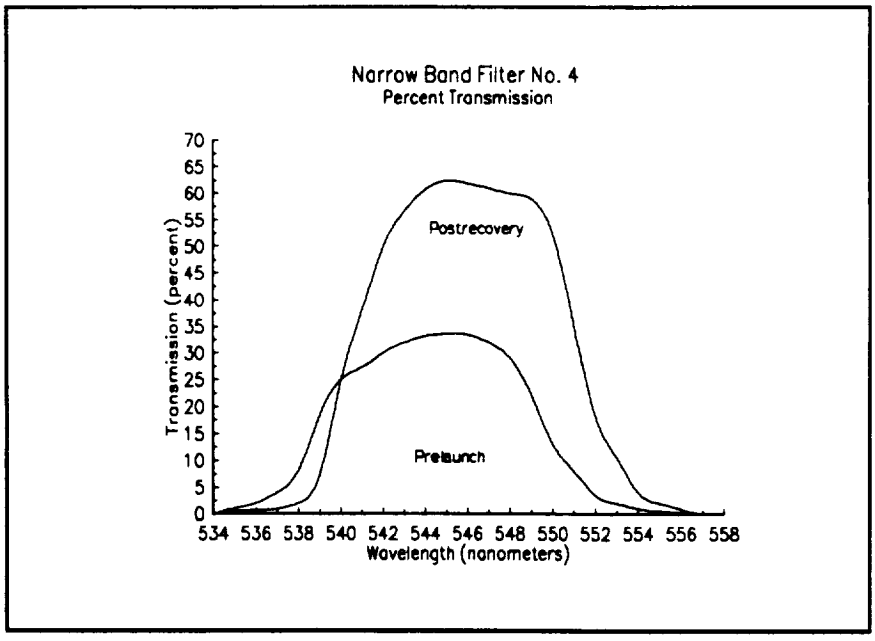

Figure 9. Prelaunch And Postrecovery Transmission Of Narrow-Band Filter Number 4.

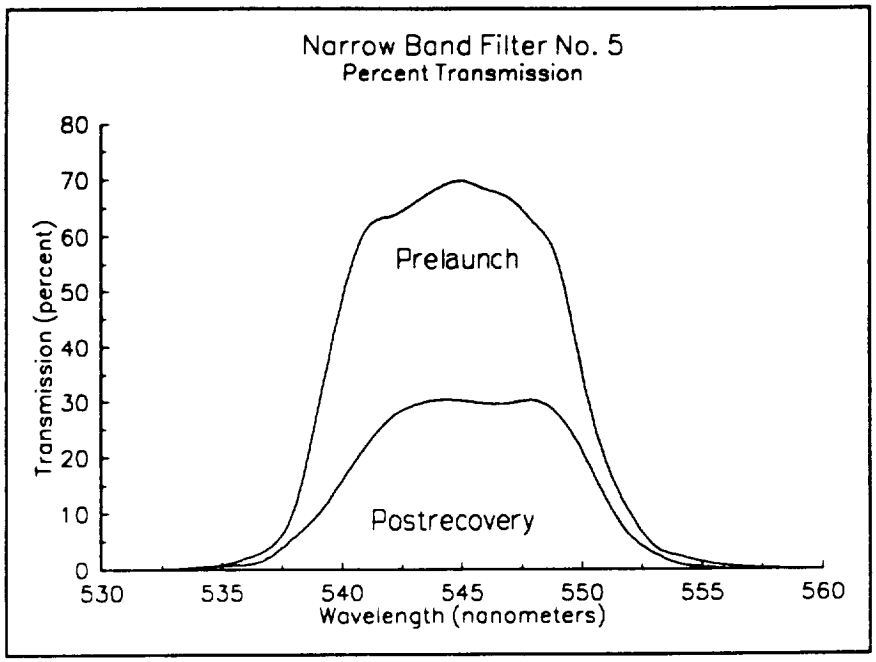

Figure 10. Prelaunch And Postrecovery Transmission Of Narrow-Band Filter Number 5.

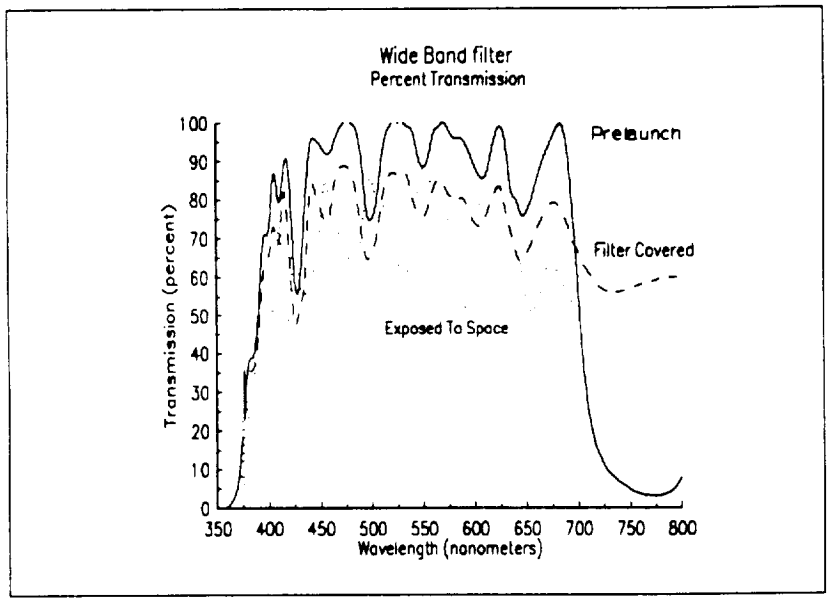

Figure 11. Prelaunch And Postrecovery Transmission Of Two Infrared-Suppression Filters. Filter Number 9 Was Under An Aluminum Cover During The Period In And Is Shown As A Dashed Line. The Dotted Line Is The Postrecovery Transmission Of The Filter Directly Exposed To The Space Environment.

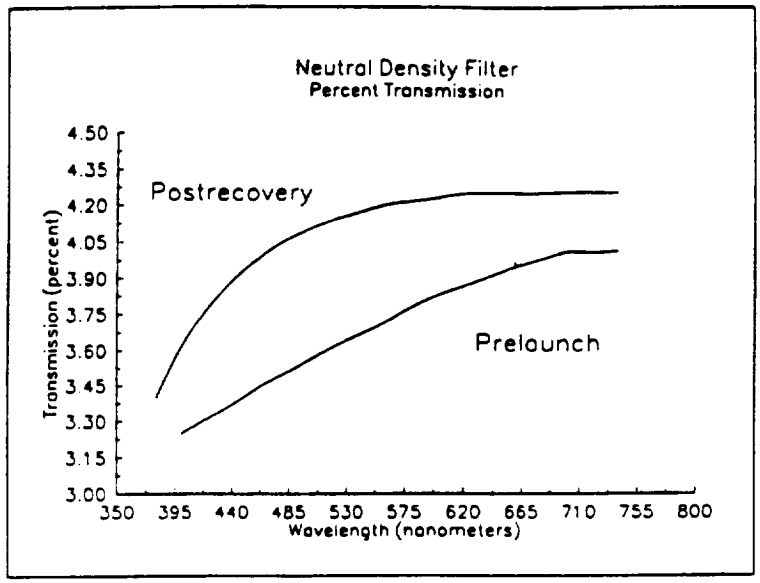

Figure 12. Prelaunch And postrecovery transmission of one of two neutral density filters. The covered neutral density filter was unchanged. The exposed filter, shown here, showed increased transmission.

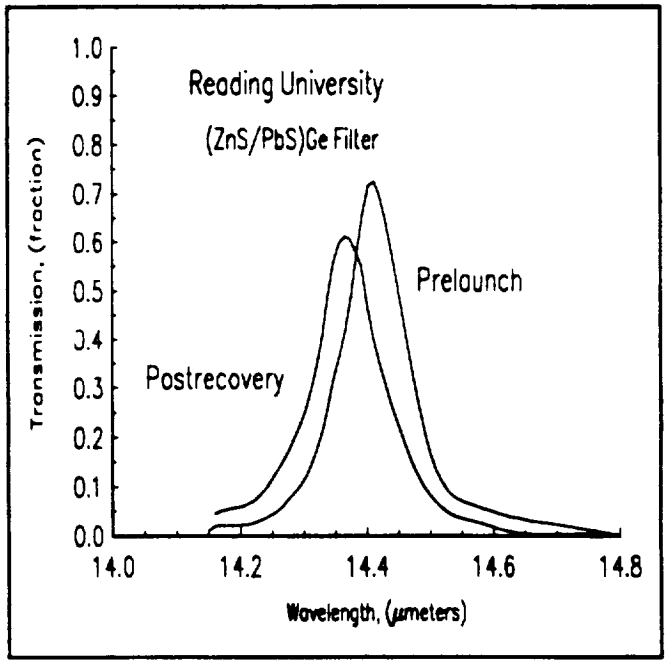

Figure 13. Prelaunch and postrecovery transmittance for one of the filters from the Reading University set (Reference 14).

Although dielectric-stack laser mirrors on the tray showed evidence of deterioration (color changes and delamination from the substrate) the appearance of the filters was unchanged except for the presence of a very thin deposited organic contamination layer. Deterioration starting from the edge and moving toward the center, often seen in aged optical filters, did not occur with the filters in this set.

A bandpass shift toward the blue may be expected if the temperature cycling causes some realignment and adjustment within the multilayer interference films which tends to decrease the average film thickness. Any external effects which disrupt or disturb the interference layer uniformity will tend to broaden the filter bandwidth[13]. The results of our rather limited set of measurements indicate that such effects tend to be small although filter number 3 is the clear exception to even this attempt at a general statement regarding these results.

Investigators at Reading University assembled a large assortment of multilayer filters on both hard and soft substrates.[14] Poor results were obtained with the soft substrates (KRS-5 and KRS-6) but postrecovery performance of the hard multilayer coatings agreed well with prelaunch measurements. Again, a slight shift toward the blue was found for narrow-band filters. Figure xx presents one example. This figure shows prelaunch and postrecovery transmission for a (ZnS/PbTe) filter on a Ge substrate. The Reading group concluded that the loss of transmission was not caused by contamination on the surface of these filters.

The reduction in narrow-band filter transmittance is the most apparent change in the performance characteristics as a result of the years in space. A reduction in transmittance occurred for all narrow-band filters including the filter under cover. We believe that reduced transmittance is caused mainly by deterioration of the cement used to attach the two filter halves together. Deterioration of plastics and other organic materials on LDEF has been noted by other NASA investigators[15] during preliminary investigations of the returned hardware. Concern with the behavior of plastics in space dates back several decades[16].

For the two near-infrared suppression (hot mirror) filters, the nearly six years of space exposure did not cause any shift in filter wavelength characteristics. However, the performance of the two filters had deteriorated. Both the transmission and the long-wave reflectance characteristics were degraded. As the results in Figure 11 indicate, the covered filter has somewhat better performance than the filter exposed directly to space. For these filters, the degradation of the interference layers and the reduced interference effectiveness are indicated by the reduced transmittance through the visible region and increased transmittance on the long-wave side. No apparent change in the filters is evident by visual observation.

The radiation exposure of less than 300 krads is below what would be expected to produce observable degradation, and the filter under the aluminum cover would have an exposure of less than one percent of this value. Yet the covered filter suffered significant degradation. The atomic oxygen fluence of $4x10^{12}/cm^2$ provides only one oxygen atom for more than ten surface atoms, insufficient to produce the observed effects. Ultraviolet irradiation would not effect the filter under cover, and normal aging of the hot mirrors should leave them in identical condition.

The thousands of temperature cycles would have nearly the same effect for the covered and exposed filters, and do not provide an explanation for the performance differences between the pair. Possible changes in stoichiometry of the ThF_4 surface layer would affect filter performance, but no major change in stoichiometry could be confirmed during our examination.

The pair of neutral density filters show somewhat different characteristics. The covered filter showed no performance changes to the accuracy of our measurements (0.1 percent detectable change in transmittance). The exposed filter showed an increase in transmittance of about one-half percent. Transmittance of this filter is shown in Figure 12. The increased transmittance is possibly the result of erosion of the inconel coating during the 69 months in low earth orbit as oxide formation should be minimal. The only physical difference noted between this pair of filters was the presence of a contamination layer on the exposed filter which stopped at the rim where the surface was covered by the attachment hardware. The small amount of contamination would reduce transmittance. Erosion would result in increased transmittance.

Several filters were cleaned with isopropyl alcohol using lens tissue after post-recovery measurements in order to determine if contamination deposited on the surface was responsible for any measurable changes in properties. The entire LDEF structure seemed covered by a yellow-brown stain of varying density which could possibly affect filter transmission. A CaF_2 window on the tray was found to have 0.2 mgm/cm^2 organic residue.[a] The source of a major portion of this contamination was traced to the black thermal control paint used in the interior of the LDEF. The deposition of the contamination was driven by temperature gradients and retention of the film on surfaces was induced by solar uv radiation.[a].

Filter number 2 had black paint along the filter edge which had begun to peel somewhat. No organic residue was found on lens tissue after cleaning. After cleaning, the transmittance of this filter was also unchanged. While in space, this filter was under an aluminum cover.

Filter number 3 showed no obvious contamination but some fogging was noted on one side which could not be cleaned off. No material was visible on lens tissue after cleaning both surfaces. The transmittance after cleaning was unchanged within the accuracy of the spectrometer.

Filter number 8, a neutral density filter, showed a faint brownish color upon reflection from its upper surface. The color appeared to be caused by a deposited nonuniform layer whose thickness varied slightly from one side of the filter to the other. The film was stubborn, but could be removed by repeated passes with lens tissue, leaving a brown stain on the tissue. This stain is consistent with the brown stain seen throughout the experiment tray surface and throughout the surface of the satellite. However, removal of the film left the filter transmittance unchanged.

As a result of these examinations, we do not find that the observed changes in filter transmittance in the visible spectral region are the result of absorption and scattering from impurities deposited on the surfaces.

The effects of erosion, compaction driven by temperature cycling, loss of volatile material from the film surface where allowable, degradation of organic materials, and contamination remain as the possible sources of the observed degradation. This combination of effects will produce results dependent upon filter design and packaging.

---

[a]Dr. Gale A. Harvey, NASA Langley Research Center, personal communication, August, 1991.

a set of mirrors arrived, fixtures were designed and fabricated to attach them to the tray. The number of mirrors to be carried on the tray varied as the program progressed and as the LDEF launch experienced delays. All mirrors were reported to be optimized for reflectance at 2.8 μm or 3.8 μm.

In the 1982-1983 period, we opened the tray container in a clean-room environment in order to review the condition of the components and possibly swap old items for improved items or replace obsolete items. At that time, it was noted that several of the laser mirrors had deteriorated. The coatings were peeling and flaking for some specimens, and pin holes and bubbles were observed in others. The group at AWFL was informed of this situation. As a result, replacement mirrors were provided. The final set of laser mirrors contained 25 laser mirrors distributed on two subtray panels. The mirrors returned to AFWL were dielectric stack mirrors similar in design to some of the filters described in the preceding section. The design of the returned mirrors used Ag plated substrates and $(ZnS/ThF_4)^n$ or $(ZnSe/ThF_4)^n$ stacks. Mirrors using the same dielectric materials were included in the final component set, and showed degradation in performance after return from space. Our limited measurements on this set of mirrors provide indications that some materials are more stable than others over time. These observations will be discussed in the following pages.

The original reflectance data for the mirrors were not supplied to GTRI, and it was assumed that the retest and analysis would be the responsibility of AFWL. When the LDEF was retrieved in 1990, there was no longer an AFWL (it had become the Phillips Laboratories) and there was no one ready to move promptly with remeasurement of the mirror properties. Accordingly, with the aid of some funds from the Space Defence Initiative Organization (through Nichols Research Corporation, Dayton, Ohio) and NASA funds, the reflectance of the mirrors was measured at Georgia Tech using a BioRad Fourier transform spectrometer.

The lack of original data and absence of construction details of the mirrors is a handicap to data analysis, but some details of construction have been obtained from the original correspondence and from Mr. Terry Donovan (NAWC, China Lake, CA) who participated in the program at the time that the original measurements were made. The data obtained from remeasurement of the mirror reflectance combined with optical filter spectral transmission data provide a better perspective on the degradation of these components than either data set alone.

Postrecovery examination of the mirrors under a microscope revealed no evidence of general peeling, flaking, or loss of adhesion by the optical coatings. Scratches and lapp marks were evident, along with residual particles (possibly of lapping compound) at the end of some of the tracks. No unusual features such as dendrite formation or major micrometeoroid impact craters were observed during surface examination. A more extensive search should reveal some impact craters as other trailing edge components exhibit such features. Don Decker of NAWC,China Lake, has examined a group of mirrors from this set. He stated that the mirrors showed evidence of an attempt at cleaning. There were also micron-sized pits on the surface that could be caused by arcing (caused by high surface potentials developed in space) or by micrometeoroid impact. In many of these mirrors, according to Mr. Decker, the surface of the mirrors would be expected to be either ZnS or ZnSe which was paired with ThF_4. These surfaces are not considered stable. These comments agree with our observation that the mirrors with the

zinc salt/thorium fluoride construction tended to deteriorate in storage as well as in space. We are unaware of any attempt at cleaning, as the mirrors were stored before mounting on the tray without changing their original packaging or cleaning them in any way.

5.3.3 Mirror Performance

The measured spectral reflectance of the mirrors contain artifacts arising from absorption caused by water vapor and other gas molecules in the optical path as well as by contamination on the mirror surface. The measured background using an aluminum mirror is compared with the reflectance of each mirror. Depending upon the time allowed to purge the system of water vapor, the resulting measurements can vary somewhat from run to run. Vibration bands for some potential contaminants are listed in Table 6.

TABLE 6

MOLECULAR VIBRATION BANDS

Molecule	Wavenumber (cm^{-1})	Wavelength (μm)
CH_2	2870	3.48
CH_3 stretch	2930	3.41
CH_3 stretch	2960-2970	3.38-3.37
H_2O	3125, 3400-4000	3.2, 2.94-4.00
	1400-2000	7.14-5.00
CO_2	2350, 3660, 2326, 3704	4.255, 2.73, 4.30, 2.70

Table 7 provides a list of the 25 mirrors, their appearance, their markings (if any), their design wavelength, and (for a few examples) their construction. Figures 14 to 20 show spectral reflectance for the seven samples whose design has been determined (mirror numbers 2,3,4,5,6,9, and 22). Spectral reflectance data for filter number 1 are also included as Figure 21. This filter was especially interesting because it had two sections, each filling half the area, separated along a diameter. One side of this filter was bright and reflective, the other was dark. The dark half was 1.8 μm thicker than the bright half, and had higher visible-light reflectance.

The construction of each filter is indicated on the figure where the construction is known. As mentioned above, this set of laser mirrors was optimized for high reflectance at either 2.8 or 3.8 μm (2632 and 3571 wavenumbers). The reflectance for the mirrors as originally fabricated would be above 99% at one of these wavelengths.

or 3.8 μm (2632 and 3571 wavenumbers). The reflectance for the mirrors as originally fabricated would be above 99% at one of these wavelengths.

The figures show artifacts in spectral reflectance due to organic materials on the mirror surface, and CO_2 and water vapor in the spectrometer optical path. Allowing extra time for the flowing nitrogen gas to purge water vapor and other gases from the spectrometer would eliminate or reduce such effects. In our case, these effects will not hinder our interpretation of the data.

The method of attaching the mirrors to the LDEF tray was to capture them between fiberglass-epoxy strips using silicone rubber washers to allow for thermal expansion. As a result, the edges of the mirrors were not directly exposed to space. The area under the washer was protected from UV radiation and erosion. Only the center of the mirrors were directly exposed to the space environment. Reflectance at the edge of these mirrors is often different than reflectance at the center. The center may have either higher or lower reflectance. Fig. 21 shows mirror number 1 where the exposed center had a lower reflectance than the rim. In Fig. 20, mirror number 22, the center had a higher reflectance than the rim. The mirror rim is subject to contamination by volatile residue coming from the thin silicon rubber gasket, while the center was subject to ultraviolet radiation, erosion and pitting from dust, and direct radiation effects.

Most mirrors in this set show a five to twenty percent drop in reflectance assuming that the original reflectance was close to one hundred percent at the design wavelength of 2.8 μm or 3.8 μm. While absolute reflectance in these measurements should be in error by a few percent caused by aging of the calibration standard, relative reflectance between different mirrors should be accurate to better than one percent.

As with the optical filters aboard LDEF, small changes at the interface between layers in the multi-layer films can result in changes in spectral characteristics and loss in performance. The source of the changes may be interdiffusion at the interface between the layers, erosion at the surface, and damage in the layers from the particulate radiation falling on the films. The actual amount of change will vary with the materials and physical construction of the stack. From the results seen in the mirrors and filters in this experiment, the conventional ZnS/ThF_4 construction does not seem as suitable as some of the other material combinations shown in this set of figures.

Some of the other material combinations are preferable to ZnS/ThF_4 as judged solely by the results of the space exposure aboard the LDEF. The Si/SiO performed better, and the Ge/ZnS pair was the best performer in this limited set of measurements.

Similar observations regarding the effects of space exposure on the optical performance of metal mirrors with and without protective coatings and multilayer high-reflectance mirrors were reported at the Third LDEF Post-Retrieval Symposium in November, 1993.** Extensive and detailed examination of mirror surfaces was reported in these papers. Oxidation and sputtering of surfaces of metal mirrors was observed, as well as interdiffusion between layers in multilayer mirrors and segregation of water molecules at interfaces.

** H. Herzig and C. M. Fleetwood, Jr., "Effects Of The LDEF Orbital Environment On The Reflectance Of Optical Mirror Materials, and T. Donovan, K. Klemm, L. Johnson, R. Scheri, J. Erickson, and F. di Brozolo, "Effects Of Low Earth Orbit On The Optical Performance Of Multilayer Enhanced High Reflectance Mirrors," Third LDEF Post-Retrieval Symposium, Williamsburg, Virginia, Nov. 8-12 (1993).

TABLE 7.
LIST OF LASER MIRRORS FROM THE AOSCE EXPERIMENT ON LDEF

FLIGHT No.	SUBSTRATE MATERIAL	COLOR OF MIRROR	NOTES (ID # if marked) [Design λ if known] CONSTRUCTION IF KNOWN Notes
1.	Metal		Silver/Grey, two semicircles, yellow rim, dark half 1.8 μm thicker. (M-8)
2.	Metal		Pale yellow, rim region is colorless. (E-8, 78041-40, M-14). $Ag(Si/SiO_x)^n$
3.	Metal		Pale Gold,rim is brighter/lighter. [2.8 μm] (78041-371). $Ag(ZnS/ThF_4)^n$, R = 99.7 (2.6-3.0 μm).
4.	Metal		Bright Yellow,Scratched.(78219-10). [3.8 μm] $Ag(ZnSe/ThF_4)$.
5.	Metal		Olive, Blue Rim. See #6. (78041-4G N). [2.8 μm], $Ag(Si/SiO)^n$
6.	Metal		Olive, Blue Rim. $Ag(Si/ZnS)^n$. R = 99.8 %. [2.8 μm] (2.6-3.0 μm), Scatter = 5.63×10^{-9}. (401 78124-05).
7.	Metal		Gray Center, Olive Rim (or Pink, Pale Green). (#278).
8.	Metal		Pale Yellow, Clear Rim (see #2). (S 731).
9.	Metal		Clear all over, slight yellowing in center. [3.8 μm]. 78219-05). $Ag(ZnS/ThF_4)^n$.
10.	Metal		Rose-Pink, Center similar in color. No #. (see #22).
11.	Metal		Aqua-Blue, Purple Rim (see #12). (#283).
12.	Metal		Aqua-Blue, Purple Rim (see #11). (#154).
13.	Quartz		Gold Color is uniform throughout (see #15). (U2A3).
14.	Quartz		Faint Yellow, Brown streaks, darker half-disk about 7-μm thicker. (No #).
15.	Quartz		Gold Color is uniform throughout (see #13). (No #).
16.	Quartz		Gold Color, Blue Rim. U2F2.
17.	Metal		Light Yellow, Clear Rim (see #2). (No #).
18.	Metal		Dark Orange, Lighter Rim, Tiny Speckles. (UIB3).
19.	Metal		Light Yellow, Clear Edge, (see #2). (No #).
20.	Metal		Al-like, Yellow at Rim, Scars (1 large). (#23).
21.	Metal		Light Yellow, Clear Rim (see #2). (No #).
22.	Metal		Magenta, Blue-Green Ring, Gold Rim, Magenta Outer Rim. (78171-17) [3.8 μm] $Cu(Ge/ZnS)^n$. See #10.
23.	Quartz		Rose, Orange Rim. (U266).
24.	Quartz		Faint Yellow, Uniform in Color, Scars. (No #).
25.	Metal		Blue-Green, Uniform in Color, Scars, Red Rim. (#59).

Note: Mirrors were mounted on the LDEF between fiberglass-epoxy boards using silicone-rubber washers. Thus, the rim of each mirror was not directly exposed to space. As a result, the rim of many mirrors shows a different interference color than the mirror center.

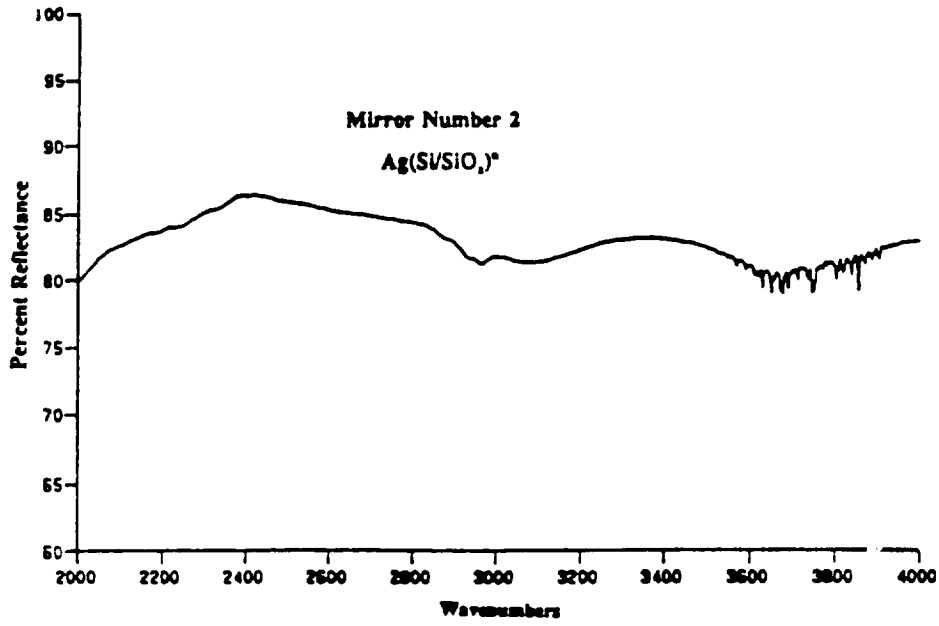

Figure 14. Postrecovery reflectance for mirror Number 2. Construction of the mirror is indicated on the figure. Absorption of water vapor affects measured reflectance at higher wavenumbers.

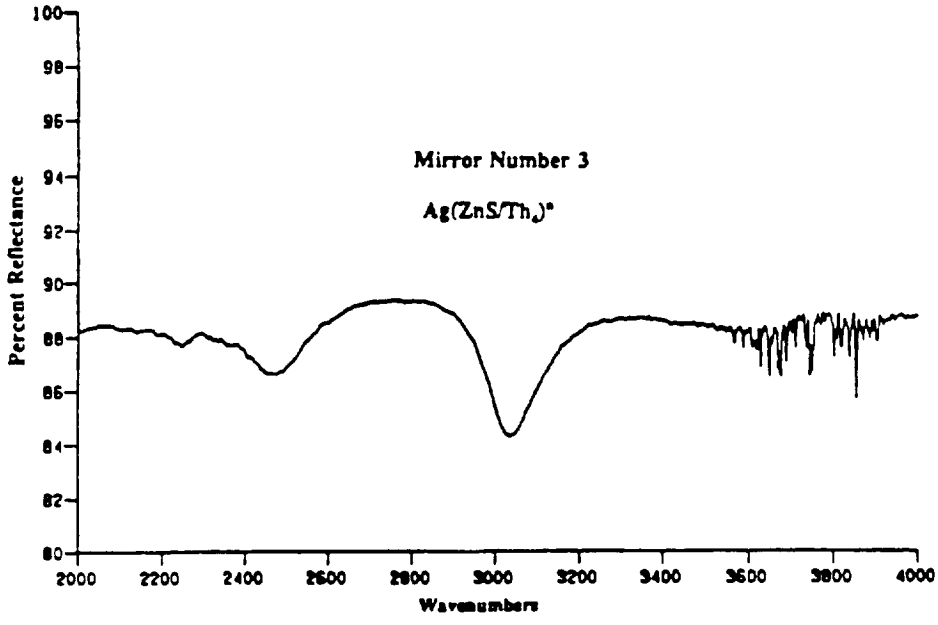

Figure 15. Postrecovery reflectance for mirror Number 3. Construction of the mirror is indicated on the figure. Absorption of water vapor affects measured reflectance at higher wave numbers.

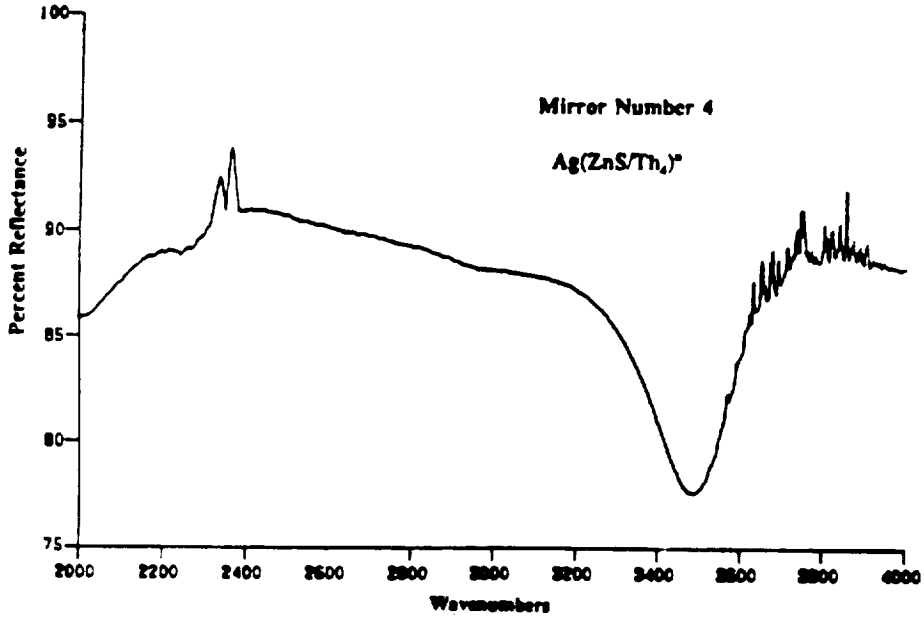

Figure 16. Postrecovery reflectance for mirror Number 4. Construction of the mirror is indicated on the figure. Absorption of water vapor affects measured reflectance at higher wave numbers along with a CO_2 doublet near 2350 cm^{-1}.

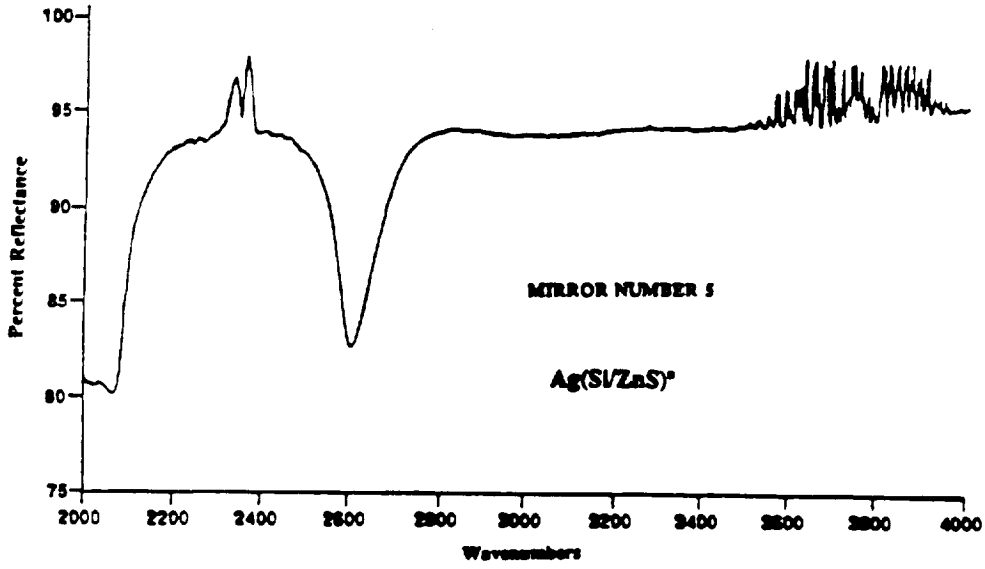

Figure 17. Postrecovery reflectance for mirror Number 5. Construction of the mirror is indicated on the figure. Absorption of water vapor affects measured reflectance at higher wave numbers along with a CO_2 doublet near 2350 cm^{-1}.

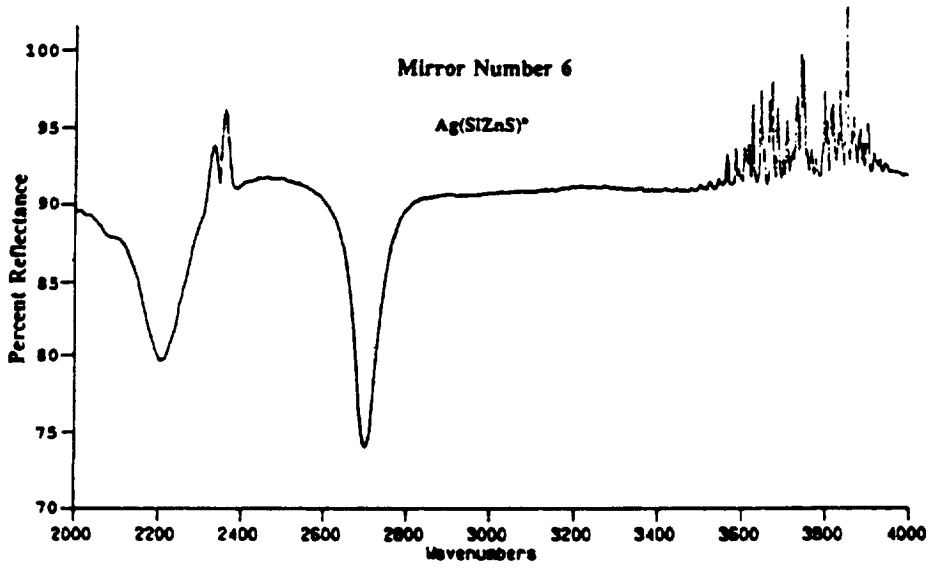

Figure 18. Postrecovery reflectance for mirror Number 6. Construction of the mirror is indicated on the figure. Absorption of water vapor affects measured reflectance at higher wave numbers along with a CO_2 doublet near 2350 cm^{-1}.

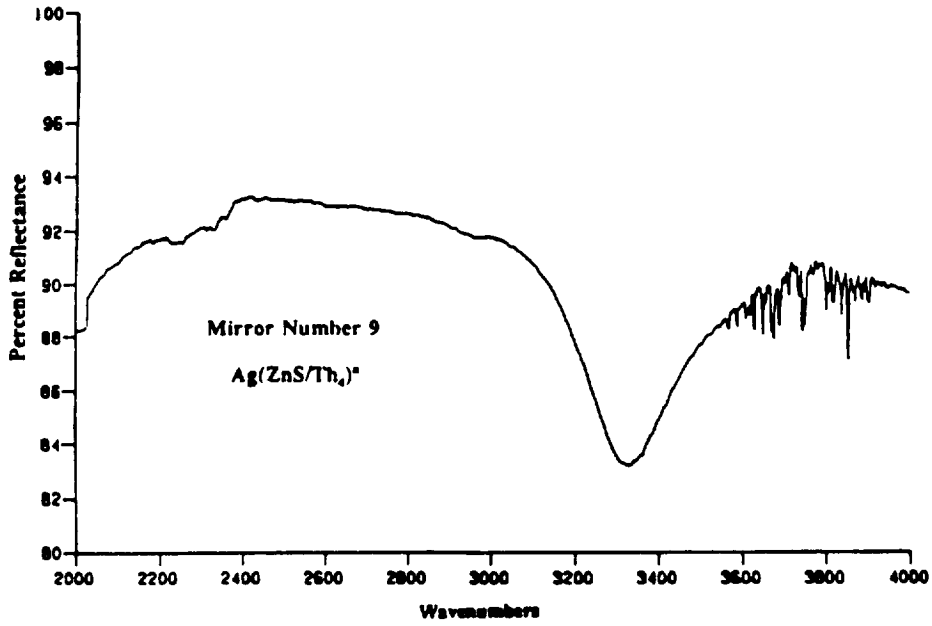

Figure 19. Postrecovery reflectance for mirror Number 9. Construction of the mirror is indicated on the figure. Absorption of water vapor affects measured reflectance at higher wave numbers along with a CO_2 doublet near 2350 cm^{-1}.

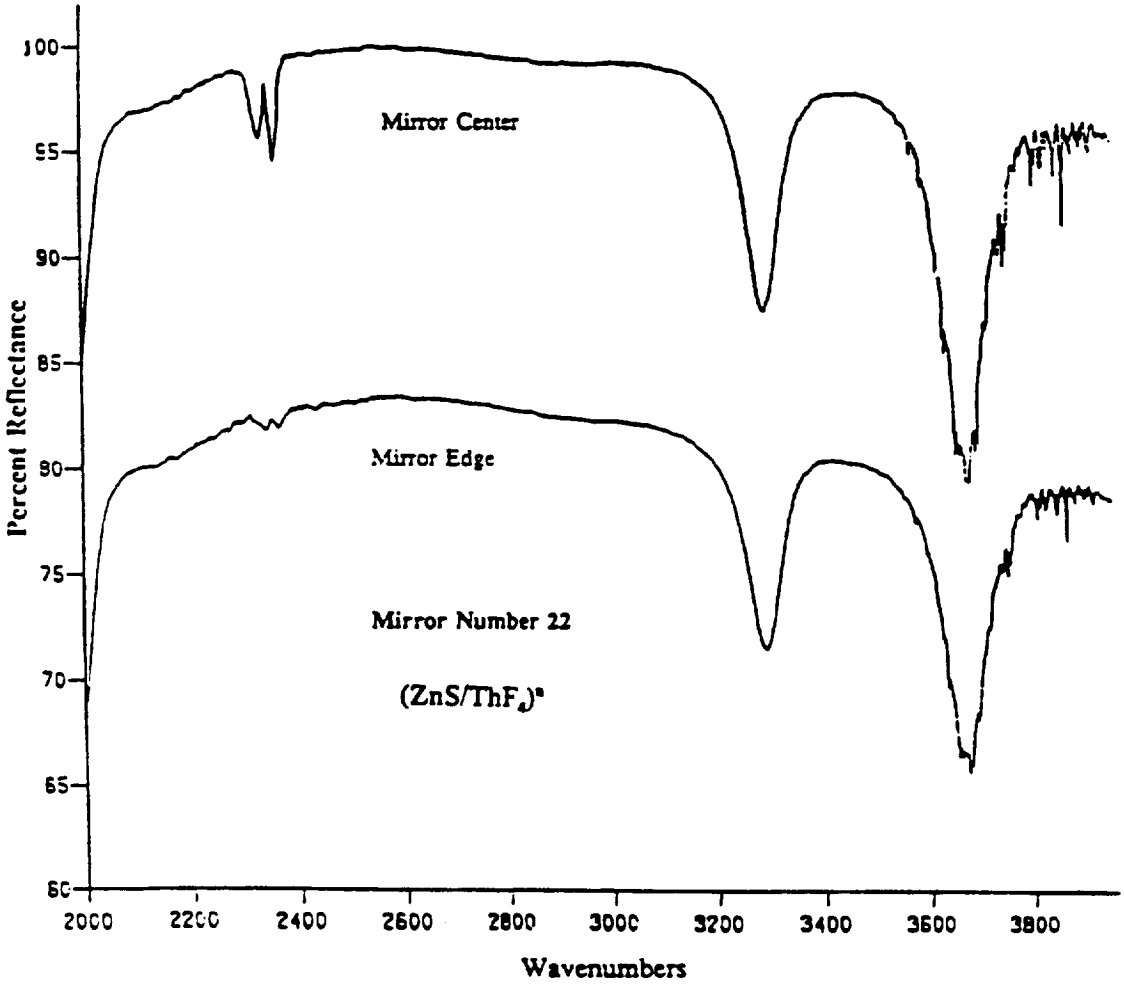

Figure 20. Postrecovery reflectance for mirror Number 22. Construction of the mirror is indicated on the figure. Absorption of water vapor in the path affects reflectance at higher wave numbers, and absorption from a CO_2 doublet appears near 2350 cm^{-1}.

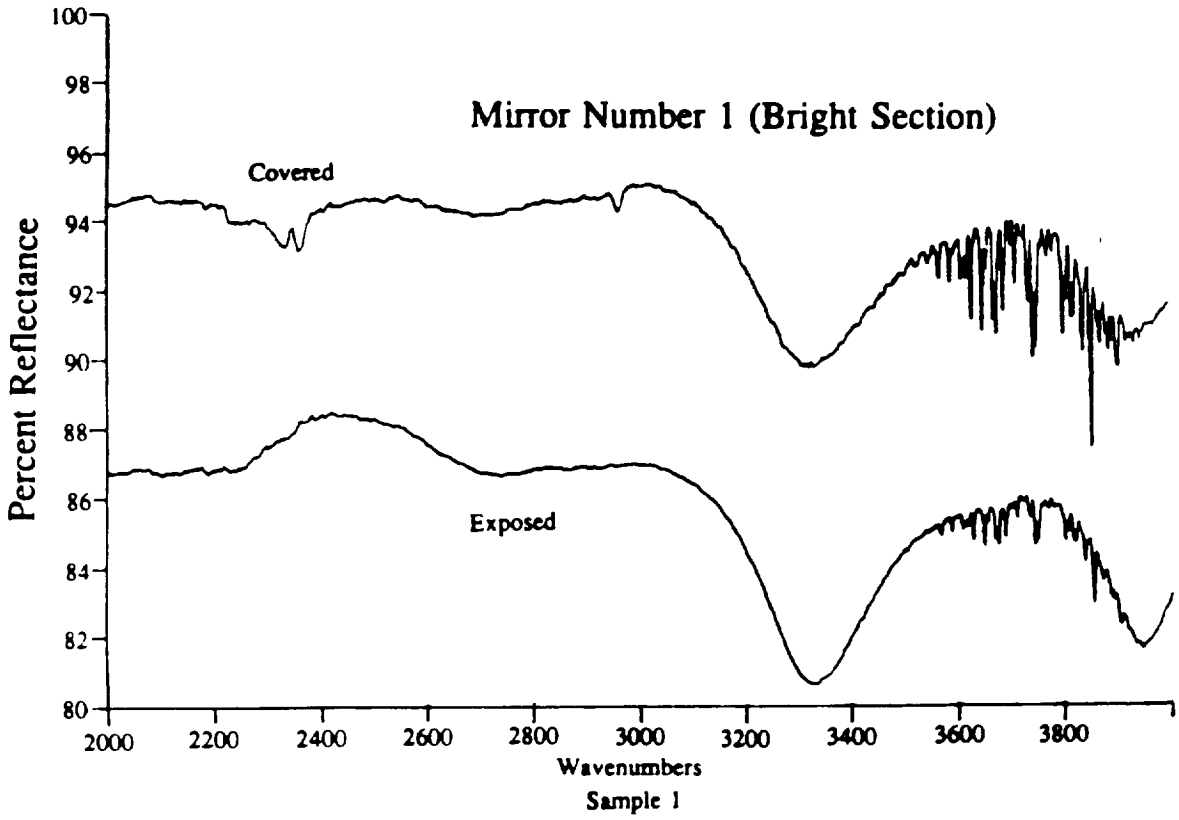

Figure 21. Postrecovery reflectance for the bright section of mirror Number 1. Absorption of water vapor and the 2350 cm^{-1} CO_2 doublet affect measured reflectance. This mirror had a bright half-disk and a dark half-disk of 1.8 μm greater thickness.

The mirrors which were returned to AFWL in February, 1983, had deteriorated while mounted in the LDEF tray and stored under dry benign conditions. These filters included the $ZnSe/ThF_4$ and ZnS/ThF_4 combinations. Other mirrors (and optical filters) using these materials formed part of the final component set. These materials resulted in degraded component performance in all cases where the materials could be identified. Other material combinations performed better.

Table 8 compares the measured mirror reflectance at 2.8-μm (3571 cm^{-1}) and 3.8-μm (2632 cm^{-1}), the wavelengths at which the designs were optimized. Filters 4 and 9 were designed for high reflectivity at 3.8-μm. Filters 3,5, and 6 were designed for high reflectivity at 2.8-μm. Donovan *et al*[17] have noted an apparent shift of the high reflectance band to higher wavelengths in their dielectric mirror measurements. In some cases, similar shifts in reflectance appear to be evident in the reflectance spectra of this set of mirrors. For example, for mirror No. 3 the peak at 2800 cm^{-1} could represent a shift from the original design peak at 2632 $^{-1}$. For a mirror fabricated from more stable materials such as mirror No. 22, the peak reflectance remains near the design wavelength of 2632 cm^{-1}.

TABLE 8

PERCENT REFLECTANCE AT 2.8μm AND 3.8 μm

Mirror Number Number	Construction	Reflectance At 3.8 μm	Design At 2.8 μm	Wavelength
2	Ag(Si/SiO)	85.0	83.3	2.8 μm
3	$Ag(ZnS/ThF_4)$	88.8	88.1	2.8 μm
4	$Ag(ZnSe/ThF_4)$	89.5	80.3	.8 μm
5	Ag(Si/SiO)	89.9	90.3	2.8 μm
6	Ag(Si/ZnS)	88.6	91.4	2.8 μm
9	$Ag(ZnS/ThF_4)$	92.9	88.25	3.8 μm
22	Cu(Ge/ZnS)	99.8	96.3	3.8 μm

VI. ANALYSIS OF FILTER AND MIRROR PERFORMANCE

6.1 Discussion

Transmittance and reflectance measurements for optical filters and mirrors from different sources exposed to the space environment for five years and nine months aboard the NASA LDEF satellite indicate several types of performance degradation.

Narrow-band interference filters show evidence of reduced transmittance, shift of center wavelength, and bandpass broadening. The shift of center wavelength toward the blue is observed for filters designed for both the ultraviolet and visible spectral regions. The magnitude of the shift is only a few nm of wavelength which will be unimportant is many cases, but can be significant where narrow-band energy is to be detected. Reduction in transmittance is not consistent for filters of different physical construction. Filters in the GTRI set, protected by cover glasses, experienced greater losses in transmittance than filters without a cover glass. Deterioration of the cement or varnish used to attach the cover glass is believed to be a major factor in the increased transmittance loss for these filters.

The standard multilayer narrow-band dielectric filter or mirror consists of alternate quarter-wave layers (optical thickness) of high- and low-refractive index materials. The process of refinement consists of varying the thickness of individual layers to optimize the design for a specific set of parameters. The final design may then make use of layers that are not quite a quarter-wave thick. For typical filter designs using quarter-wave stacks of paired layers, approximate relations for filter bandpass and reflectance can be obtained.

$$\Delta\lambda/\lambda = (8/\pi)(n_L/n_H)^{2m}$$

where

λ is the design wavelength,

$\Delta\lambda$ is the half-width of the spectral transmittance band,

m is the number of high-low index dielectric layer pairs,

and n_H and n_L are the refractive indices of the high- and low-index dielectric materials used to construct the filter.

For the reflectance of a quarter-wave stack, a similar approximation can be obtained.

$$R = (n_H^{2m} - n_L^{2m})/(n_H^{2m} + n_L^{2m})$$

where all quantities have their previous definitions.

High internal reflectance of the individual layers of the filter (or mirror) gives rise to the narrow bandpass.[18] The small changes in bandpass indicate some reduction in the internal reflectance of the layers. The changes in reflectance could result from interdiffusion of the layers of varying composition and refractive index which would be equivalent to index changes of a few parts per thousand. The resulting reduced gradient in refractive index across the layer pairs reduces the reflection coefficient between the layers. Moreover, these small reductions are consistent with the loss of transmittance for filters without a cover glass. Similar considerations apply to the performance changes in multi-layer dielectric-coated mirrors.

As an example, the characteristics of the GTRI filter 1 (Fig. 6) are consistent with a design using a double set of 7 pairs of ZnS/Cryolite layers with a half-wave spacer.[19] Using the relationships described on the previous page, the shift in peak wavelength toward the blue of 1 nm corresponds to a decrease of average layer thickness of less than 0.2 nm, or less than 1/50 Å. For this filter, the increase in bandpass width of 0.2 nm corresponds to a change in reflectance of the layers in the stack of 3 parts per 1000. These changes appear reasonable considering the construction and dimensions of these narrow-band filters.

Infrared suppression filters (hot mirrors) showed a reduction in transmittance and evidence of deterioration of the interference layers as a result of space exposure (Fig. 11). These filters combine a low-pass and high-pass filter design to produce the desired spectral characteristic. The filter under cover experienced a similar but a smaller amount of degradation compared to the exposed filters.

Broader and deeper cycles in spectral transmittance indicate the magnitude of these effects. No cement was used in the construction of these filters. Temperature cycling, dimensional changes, erosion, changes in surface stoichiometry, and contamination are possible sources of the deterioration.

Direct exposure to the space environment causes enhanced degradation over normal ageing and degradation in a covered space environment. The direct exposure to ultraviolet radiation and the natural ionizing radiation environment may provide the necessary energy to advance the rate of normal atomic rearrangements in the layers which are implied by the changing optical properties.

Neutral density filters are of different construction and reacted differently to the effects of space exposure. The sample exposed to the space environment had slightly increased transmittance (0.5%). The covered sample was unchanged. A small amount of erosion of the metal film of a few percent of the film thickness would be sufficient to cause the observed increase in transmittance.

Atomic oxygen exposure of the films while in orbit represented about one oxygen atom per hundred surface atoms; insufficient flux to produce the observed changes in the GTRI filters. Less than 300 krads of ionizing radiation reached the tray surface which is well below the level where previous studies have indicated that radiation effects begin to appear. Only 1% of this flux reached the covered filters which suffered similar degradation effects.

All filters were about the same age, so temporal effects should have the same effect on similar filters. Erosion and contamination are difficult to quantify, yet must also be considered as a possible source of the differences between exposed and covered filters.

Consideration of the data for the filters, mirrors, and detector windows leads to the following speculations regarding the physical phenomena that are believed to be the major causes of the observed degradation in the collection of optical filters aboard the LDEF. Again, similar considerations apply to the set of laser mirrors.

Narrow-Band Filters (Three Effects)

Drop in Transmittance

Degradation and ageing of the cement or varnish used to attach the cover glass by UV and other radiation increases opacity and reduces throughput. Smaller effects are observed in filters with no cover glass, indicating deterioration of the sharp interface between deposited layers, and the resulting reduced interlayer reflectance (depends upon fabrication technology).

Band-Pass Shift

Years of temperature cycles (>32000) in orbit and normal ageing of control filters increase packing density and reduces average filter-layer thickness which causes a band-pass shift toward the blue (depends upon materials and fabrication technology)

Band-Width Increase

Temperature driven interdiffusion between the interference layers reduces interlayer reflectance and increases filter bandwidth (depends upon materials and fabrication).

Wide-Band Filters (Two Effects)

Disruption of Design Tolerance

As with the narrow-band filters, compaction and interdiffusion disrupts the design balance and reduces the design effectiveness causing degraded cutoff slope and deeper and wider ripples in the transmittance spectra.

Drop In Transmittance

The reduced reflectance not only degrades the design, but also contributes to reduced transmittance. Thus, even the hot mirror under cover suffered reduced transmittance. In addition, an exposed filter may have experienced erosion and contamination at the exposed surface causing additional transmittance loss.

Neutral-Density Filters (One Effect)

Increase In Transmittance

The slight increase in transmittance for one exposed filter was likely caused by erosion plus a small amount of prelaunch and postrecovery oxidation. The similar covered filter may have a slight (less than 0.1%) increase in transmittance due also to oxidation.

The importance of such physical phenomena to degradation of multilayer filters and mirrors in the low-earth-orbit (LEO) environment was not appreciated in the early 70's, and specific experiments to quantify these effects in an orbiting satellite have not been designed. In order to provide conclusive support for our proposed explanation for the measured filter degradation, additional studies are required (for example, additional LDEF missions). Neutral-density filters could be exposed in space and checked specifically for oxidation and erosion which would lower the optical density. Experiments designed to detect possible loss of halide from compounds such as MgF_2, ThF_2, and $ThBr_2$, could be developed. Structures such as substrates alone and substrates with one or two pairs of high/low refractive index materials could be used to look for loss of halide (or certain other) components, compaction of the layers, and interdiffusion between layers.

Filters of the same general composition from different manufacturers could be compared to determine the effect of different manufacturing processes on stability in the (LEO) environment. Now that these specific degradation mechanisms have been proposed, experiments designed specifically to investigate them are possible. For example, experiments to compare filters with similar performance but constructed with either all hard or all soft materials would provide a quantitative measure of performance differences. In the meantime, care should be exercised in filter selection for space-borne systems where these observed degradation effects could occur.

It has been suggested that improvements in filter manufacture during the years since the 1970's should reduce any observed degradation in the filters using older technology from the LDEF era. The major effects mentioned here *are not eliminated* by better vacuum during manufacture, purer raw materials, and novel deposition techniques. Improved deposition and annealing may reduce the tendency toward tighter packing caused by normal ageing and by temperature cycling in orbit. However, any improvement in this area remains to be demonstrated.

While the discussion in the preceding paragraphs has been concerned primarily with multilayer dielectric optical filters, similar consideration apply to multilayer dielectric mirrors because the construction techniques and materials are similar. Consequently, degradation effects should be, and are found to be, similar. However, for mirrors, as well as filters, designed for the infrared region rather than the optical region, the larger layer thicknesses may change the relative effects of atomic rearrangement, ageing, and high energy radiation displacement damage. Therefore, we may expect that the effects of high-energy radiation are severe for multilayer filters and mirrors designed for the infrared region than for filters and mirrors designed to operate in the UV region. However, as noted in this report and as noted by others,*** substrates and coated mirrors also degrade.

6.2 Conclusions

The results of these experiments provide several guidelines and conclusions for the

***This statement is supported by references 4, 14, and 15.

selection and use of optical materials in space. Table 9 lists the observed effects of low-earth-orbit space exposure on multilayer filters and mirrors from the Georgia Tech set and the reported effects of other experimenters for similar components.

TABLE 9.

CONCLUSIONS REGARDING MULTI-LAYER FILTERS AND MIRRORS

For irradiation levels under 1/3 Mrad, degradation effects from high-energy radiation are small.

Radiation-induced absorption and contamination-induced absorption in optical materials is strongest in the UV spectral region, decreasing through the visible region.

Narrow-band filters exhibit a *"Blue"* shift of 1-9 nm. Effects of compaction/densification and interdiffusion between layers perturb the design of the multilayer filters resulting in loss of performance.

Stable substrate materials are Si, SiO_2, Al_2O_3, Quartz, ULE Glass.

Suspect materials are fluorides such as MgF_2, CaF_2.

Poor substrate materials are KRS-5, KRS-6.

Contamination acquired during six years in storage and six years in space causes an increase in off-axis scattering from optical surfaces of a factor of ten over scattering from the original cleaned surface.

Direct radiation damage effects on all optical components and devices were minimal with few exceptions over the six-year period. Moreover, mounting of components typically gave maximal exposure to these optical components, so that the results of the LDEF experiments represented worst-case conditions. Additional protection from ionizing radiation can easily be provided where desirable. These results from LDEF experiments are in agreement with previous studies indicating that ionizing radiation exposures of less than 1/3 Mrad will not produce significant changes in the properties of substrate materials and optical filters. The effects of the irradiation (for both high-energy photon and particulate irradiation) on substrate and window materials make their appearance first as a reduction in ultraviolet transmission for both ionizing and photon irradiations.

Careful and thorough cleaning of all optical components and careful workmanship in fabrication will contribute to the stabilization of properties in space. Contamination deposited on optical components reduces transmittance. The effect was strongest in the ultraviolet region, and became small or undetectable in the visible and infrared regions. Shutters or other means to protect the optical surfaces through the launch and early orbit phases will be necessary to protect critical surfaces from such contamination. Surface protection seems to be essential for optical systems designed to operate in the ultraviolet region.

Multilayer narrow-band filters have the design wavelength shifted toward the blue by an amount which is small (1-4 nm), but significant in many cases. The related increase of bandwidth will depend on the materials used. Material choice is important for filters and mirrors. Soft materials are to be avoided. Zinc sulfide and thorium fluoride compounds showed degradation effects in several components, but not all.

These two compounds are commonly used as interference coatings. Materials such as Si, SiO, and Al_2O_3 showed greater stability under low-earth-orbit (LEO) conditions. Quartz and ULE glass are stable substrates, as are silicon, germanium. The materials MgF_2, and CaF_2 were suspected as being responsible for poor performance in some experiments.

Soft materials such as KRS-5 and KRS-6, which degraded in orbit in all experiments, are to be avoided. Even when coated, delamination of the coatings deposited on these soft substrates took place in the case of filters from Reading University. These two materials were unstable under low-earth orbit conditions.

Similar considerations apply to dielectric mirrors. Spectral shifts in reflectance may limit the use of such mirrors in space-based laser cavities, but well protected and temperature stabilized components may survive with minimum changes.

Further studies of these complex phenomena are desirable to assure long-term survival and operational stability of optical systems operating in the low-orbit environment.

VII. BLACK PAINTS

7.1 Introduction

Measurements of reflectance of several optical-black surface finishes, characterizing their suitability as optical-baffle coatings for sensors operating from near-infrared to near- millimeter wavelengths were completed in the late 1970's.[20,21] This work was done in cooperation with the Lockheed Missiles and Space Company where the coatings were prepared. In particular, William H. Alff and J. R. Grammer were instrumental in encouraging and supporting the activity. In order to extend the initial understanding of the optical properties of the coatings, six samples of standard black coatings were then included in the GTRI component set for exposure to the space environment for a planned six to ten month mission.

During the nearly twelve years between the initial collection of materials for the LDEF, our reflectance measurements, the satellite launch, and subsequent recovery, several other reports on infrared reflectance of optical-black surface finishes were published[22,23,24]. In other work of

interest, Smith[25,26] derived a reflecting-layer model for a dielectric film which includes both reflection and scattering. The model was fitted to reflectance spectra for seven optical-black coatings (including some materials considered here) for wavelengths extending to 300 μm. We use the Smith model to provide an indication of the parameters which change as a result of the effects of space exposure, although the model cannot easily explain our results at far-infrared wavelengths beyond about 250 μm.

Normal-incidence reflectance of optical-black coatings depends on coating thickness and surface smoothness, as well as the optical constants of the coating. We find that space exposure reduces normal reflectance in general, and significantly reduced reflectance at extreme infrared wavelengths. The results have important implications for the use of these materials for optical baffle applications in space-based optical systems.

7.2 Experimental Methods

All samples were prepared on substrates of 1-mm thick aluminum, 1.27-cm in diameter. Their pre-launch and post-recovery reflectances were measured over about 40-425 μm using a modified Grubb-Parsons Fourier-transform spectrometer.[27] In the pre-launch measurements, light-pipe optics delivered the radiation to the sample. Subsequently, the Grubb-Parsons instrument was modified, incorporating mirror optics rather than light-pipe optics to allow measurements on small samples with good control of the radiation beam. For both pre-launch and post- recovery measurements, the absolute reflectance was determined by a sample-in sample-out method, using a polished coin-silver mirror as a reference. This continual dynamic calibration of the data during measurement ensures that the differences in the spectrometer before and after the samples were exposed to the space environment does not effect the reliability of the measured reflectance spectra.

In both the before and after measurements, the radiation impinged on the samples at an angle of about 12°, negligibly different from normal incidence. In both sets of measurements, absorbing water vapor was eliminated from the spectrometer. All measurements used a Unicam Golay cell with polyethylene filtering as the infrared detector, and a commercial liquid helium cryostat with a cold finger to achieve cryogenic sample temperatures.

A far-infrared optically-pumped laser was used in the pre-launch measurements to extend the measurement range to 570 and 1217 μm. Some of these results are shown here. No such extension was carried out in the post-exposure measurements.

7.3 Experimental Results

Properties of the six optical-black coatings placed on the LDEF satellite are listed in Table 10. The thicknesses of the coatings were determined from measurements on neighboring areas.

Results of normal-incidence reflectance measurements for the six optical-black surface finishes are shown in Figures 22-25 where the wavelength is plotted on a logarithmic scale to better display the short-wavelength reflectivity. Measurements at cryogenic temperatures (near the temperature of liquid helium) indicate increased reflectance of five to ten percent where the coatings become partially transparent (wavelengths beyond one hundred μm) and negligible differences at shorter wavelengths where the films are strongly absorbing.

TABLE 10.

PROPERTIES OF OPTICAL BLACK COATINGS

Material	Manufacturer	Coating Thickness (μm)
3M Black Velvet Nextel 101-C-10	Minn. Mining & Manufacturing Co.	63
Chemglaze Flat Black Z306	Houghson Chem. Co.	53
Chemglaze Glossy Black Z302	Houghson Chem. Co.	51
Cat-A-Lac Black	Finch Paint Co.	69
IITRI Bone Black Silicate (D111)	Illinois Institute of Technology Research Institute	74
Martin Black Anodize	Martin Co.	71

Figures 26-29 present original and remeasured normal-incidence reflectance of a set of four special coatings containing acetylene prepared during the late 1970's as part of this study. These reflectance measurements provide an indication of the effect of storage in a laboratory for thirteen years on the normal reflectance of certain black paints and also provide an indication of any calibration problems arising as the result of instrument modifications during the years between measurements.

While the original data are reproduced in two cases, the remeasurement shows a slightly decreased reflectance for the sample containing 25% acetylene and a slightly increased reflectance for the sample containing 50% acetylene. The stored samples do not exhibit the striking changes that appear in the spectra of the space-exposed samples.

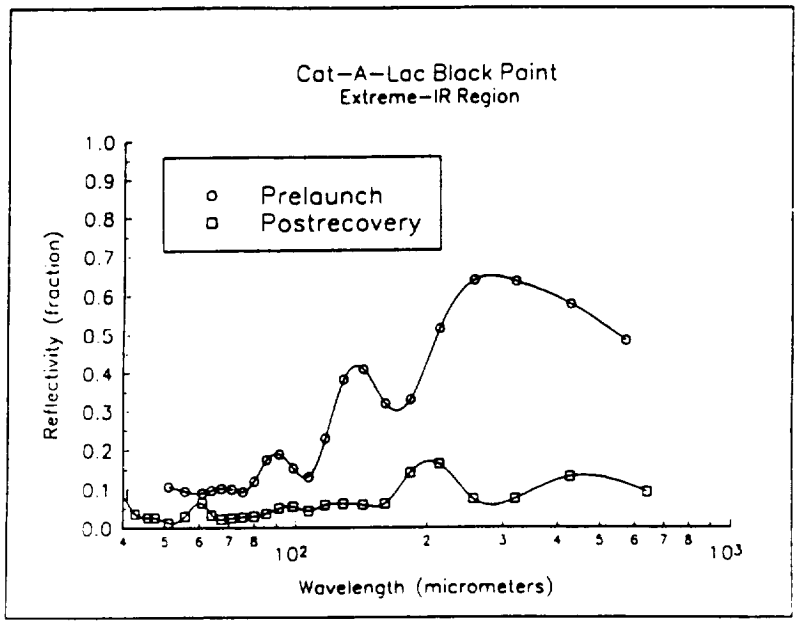

Figure 22. Prelaunch and postrecovery normal spectral reflectance of Cat-A-Lac Black from 40 to 400 μm at room temperature. Postrecovery data indicate reduced reflectance.

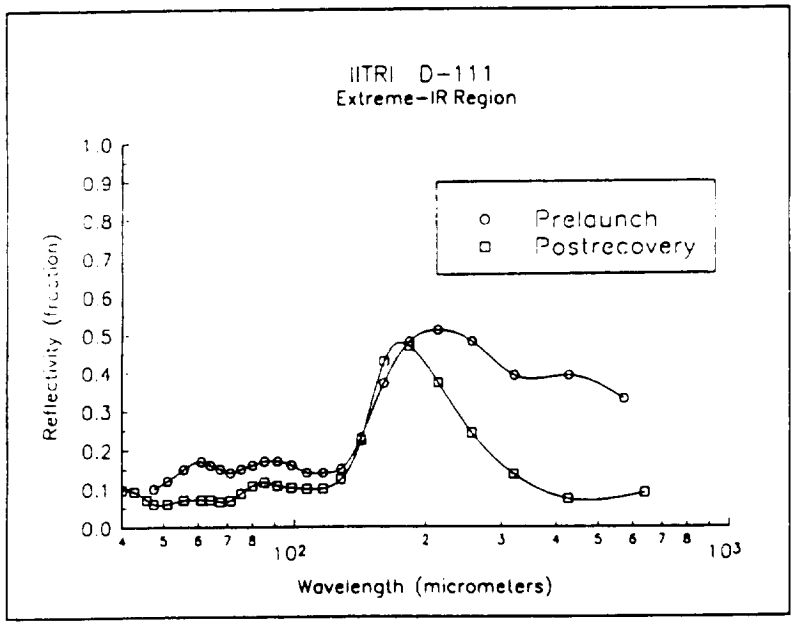

Figure 23. Prelaunch and postrecovery normal spectral reflectance of IITRI D111 from 40 to 400 μm at room temperature. Postrecovery data indicate reduced reflectance.

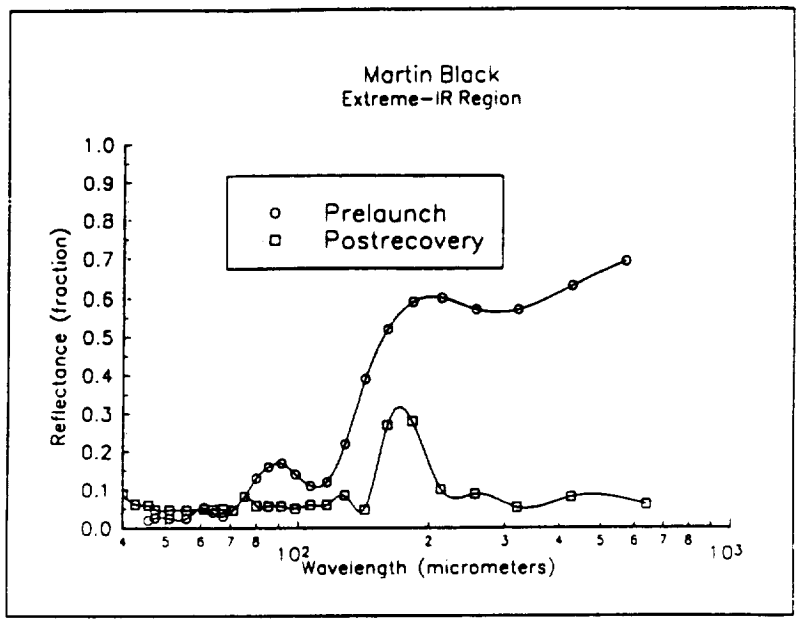

Figure 24. Prelaunch and postrecovery normal spectral reflectance of Martin Black Anodize from 40 to 400 μm at room temperature. Postrecovery data indicate reduced reflectance.

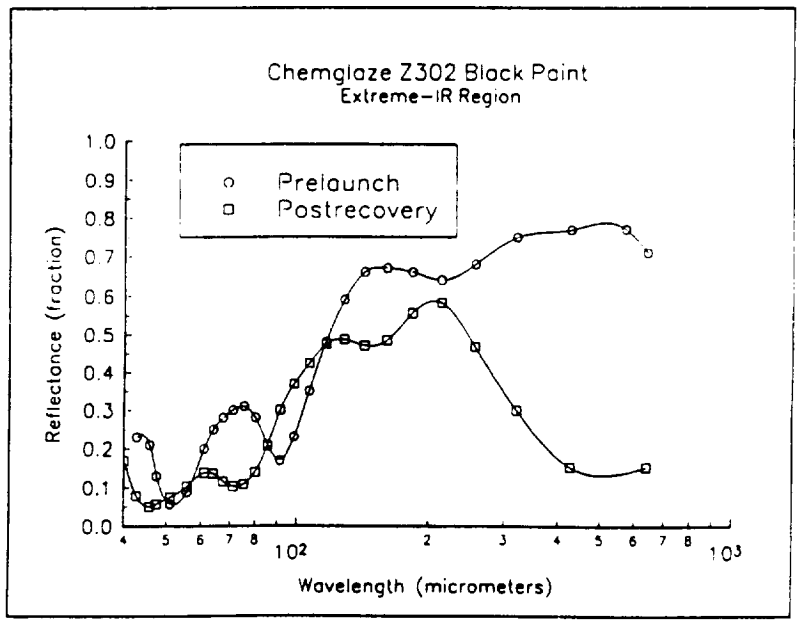

Figure 25. Prelaunch and postrecovery normal spectral reflectance of Chemglaze Z-302 Glossy Black Paint from 40 to 400 μm at room temperature. Postrecovery data indicate reduced reflectance.

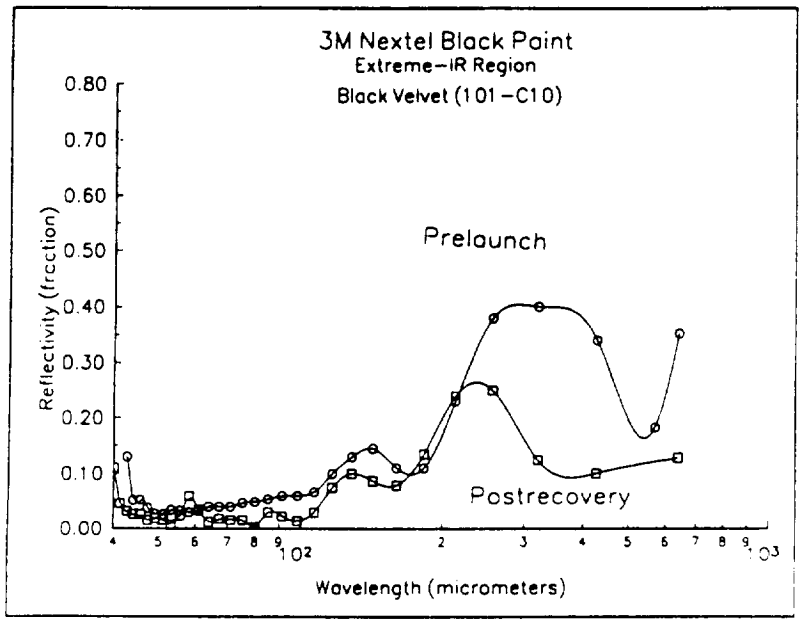

Figure 26. Prelaunch and postrecovery normal spectral reflectance of 3-M Black Velvet Paint for two thicknesses, 64 and 122 μm at room temperature. Postrecovery data indicate reduced reflectance.

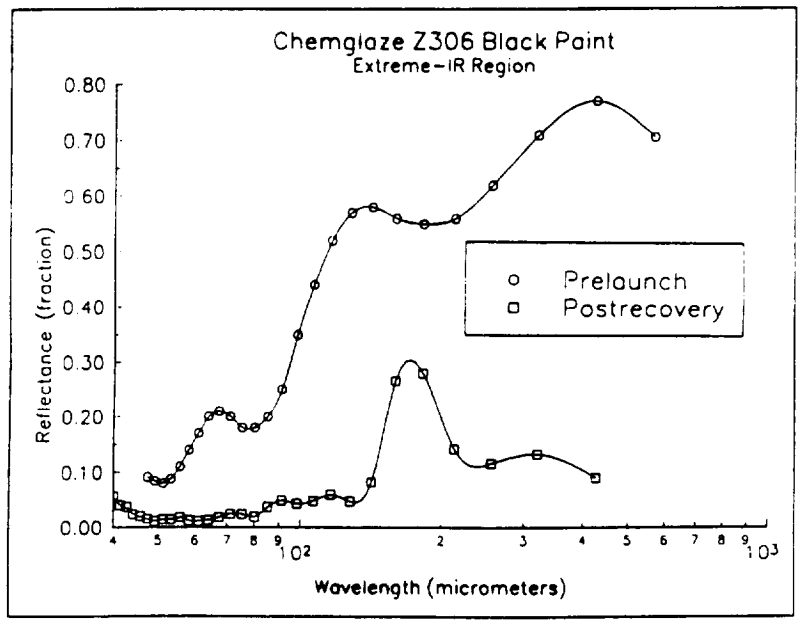

Figure 27. Prelaunch and postrecovery normal spectral reflectance of Chemglaze Z-306 Flat Black Paint at cryogenic temperatures and at room temperature. Postrecovery data indicate reduced reflectance.

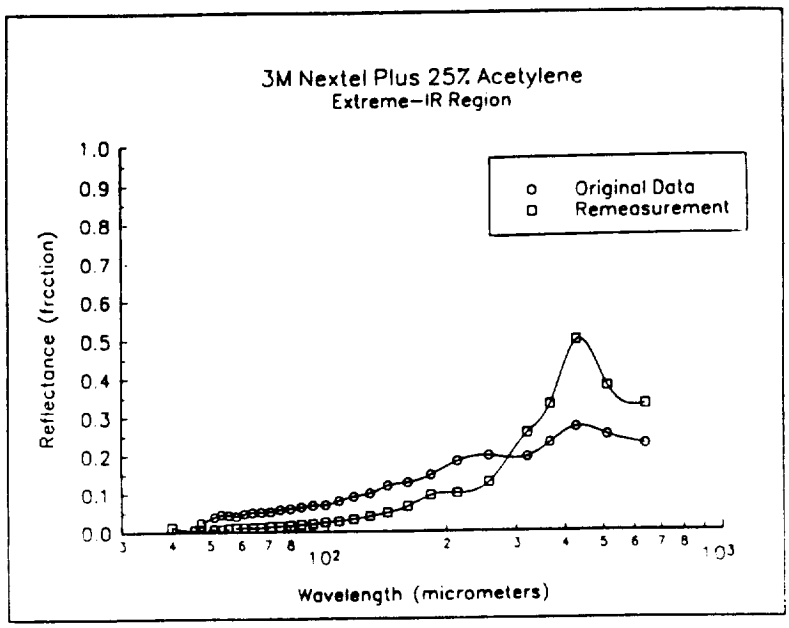

Figure 28. Original and remeasured normal reflectance for a sample of 3M paint containing 25% acetylene. Period between measurements was approximately 13 years.

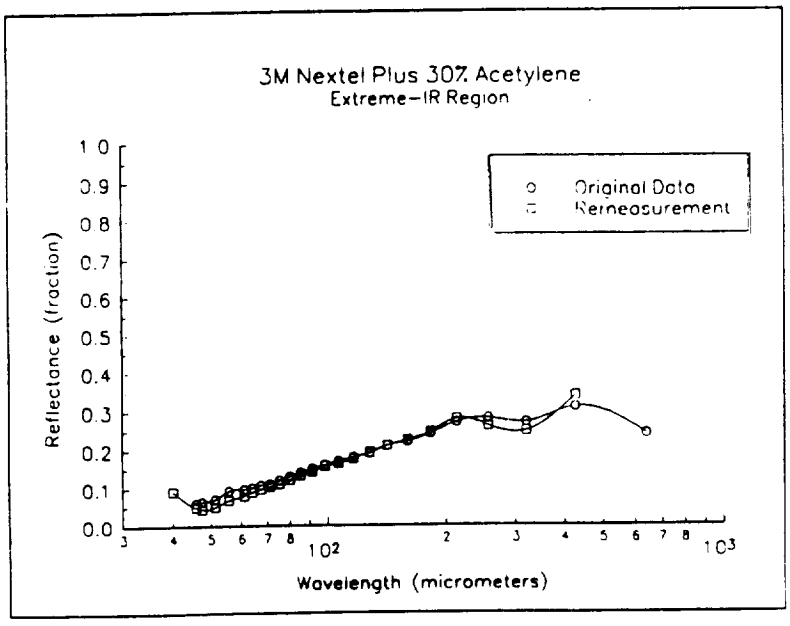

Figure 29. Original and remeasured normal reflectance for a sample of 3M paint containing 30% acetylene. Period between measurements was approximately 13 years.

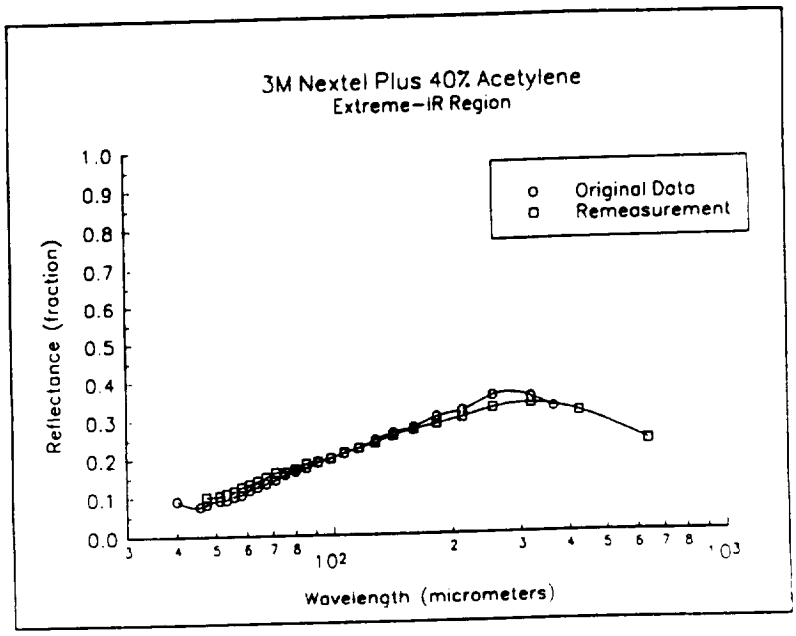

Figure 30. Original and remeasured normal reflectance for a sample of 3M paint containing 40% acetylene. Period between measurements was approximately 13 years.

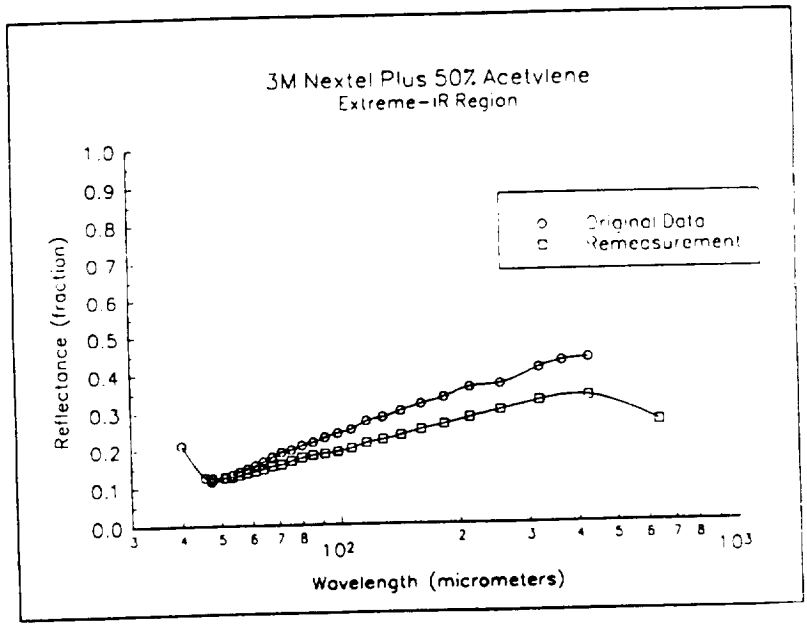

Figure 31. Original and remeasured normal reflectance for a sample of 3M paint containing 50% acetylene. Period between measurements was approximately 13 years.

The acetylene-containing samples succeed in inhibiting the rapid rise in reflectance at wavelengths beyond 100 μm which is a characteristic of the six coatings placed aboard the LDEF satellite. The intent of the acetylene additions was to reduce the contribution to the reflectance from the coating-substrate interface at wavelengths where the coatings were relatively transparent.

The most noticeable effects on the six space-exposed samples twelve years after sample preparation (including nearly six years in space) are the reduction in reflectance at all wavelengths and the trend to decreasing reflectance with wavelength beyond about 150 μm.

These changes suggest that the coatings will exhibit improved performance as optical baffles after aging and exposure in the space environment compared to their characteristics when freshly prepared. Measurements at cryogenic temperatures result in minor changes in normal reflectance for both the original measurements and the post-recovery measurements.

7.4 Analysis

The reflecting-layer model of Smith[25,26] was used to analyze the reflectance spectra. It was not possible to fit the spectra at the longest wavelengths. An example of an approximate fit to the spectra for sample Z306 is shown in Figure 32. The dotted lines represent the data, while the solid lines represent the calculated spectra. The optical parameters used for the prelaunch reflectance were those used by Smith for Z306. These parameters along with the parameters characterizing the post-recovery data are presented in Table 11. The short wavelength spectra could be reproduced, and the interference fringes could be roughly reproduced.

At long wavelengths, the model predicts a rising reflectivity as the optical depth of the coating decreases and the wavelength becomes greater than both the physical thickness of the coating and a parameter characterizing surface roughness. Theory at this level of sophistication suggests, therefore, that all dielectric materials will exhibit rising reflectance at sufficiently long wavelengths. While this is physically unrealistic, a reasonable fit at both long and short wavelengths for our samples could not be attained without allowing the optical constants to vary with wavelength. The required variations would be empirical at this time.

The postrecovery reflectance data could not be fitted with a change in surface roughness or coating thickness, indicating that surface roughening or loss of material from erosion or other effects of space dust and debris did not cause the decreased reflectance. The approximate fit to the postrecovery spectra in Figure 32 was obtained by increasing the value of the imaginary component of the index of refraction from 0.066 to 0.22 while leaving the real component unchanged.

The implication is that space exposure increases the imaginary component of the complex index of refraction for all samples resulting in increased absorption at all wavelengths. Since all six coatings show increased absorption, it is likely that there are some common effects. The typical coating consists of absorbing particles (pigment) with a binder.[28] We Speculate that the increased absorption may be related to the loss of volatile components in the binder, and the degradation of the pigment and binder by UV radiation resulting in an increased density of absorption sites in the paint films. While these effects could occur during natural ageing, space exposure may accelerate them.

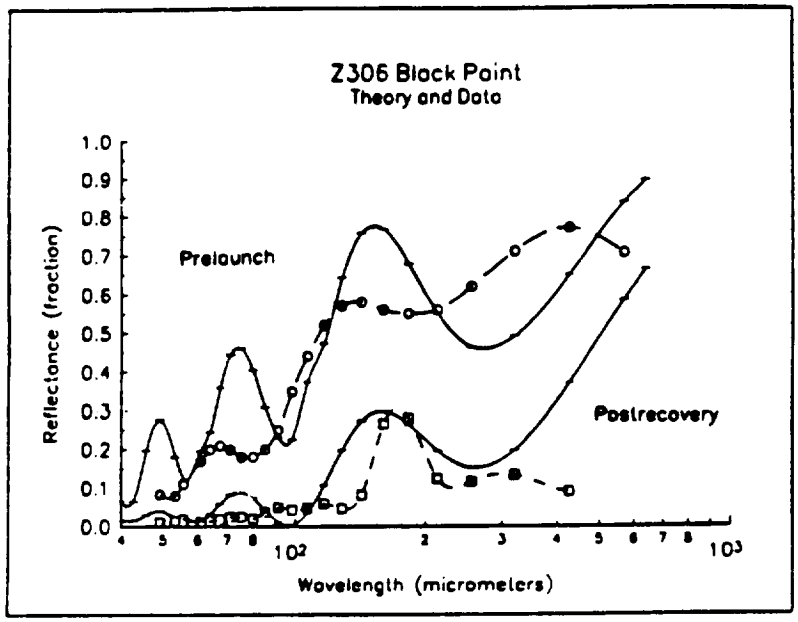

Figure 32. Comparison between reflectance data (dashed lines) and for sample Z-306 and reflectance calculated using the model of Smith[25,26] (solid lines). The calculations assume increased absorption for postrecovery data. Left pair of curves are prelaunch data; right side pair are postrecovery data. See text for details.

TABLE 11.

OPTICAL CONSTANTS AND PARAMETERS FOR ANALYSIS OF Z306 PAINT COATING

Refractive Index n = 1.37	Front Surface Roughness σ_1 = 2.3 (μm) m_1 = 1 (deg)
k = 0.066 Prelaunch k = 0.22 Postrecovery	Back Surface Roughness
Coating Thickness	σ_2 = 0.3 (μm)
d = 53 (μm) m_2 = 1 (deg)	
Coupling Parameter	Acceptance Angle
C = 4	Alpha = 0.235 (deg)

VIII. MISCELLANEOUS ACTIVE COMPONENTS

8.1 Light Modulator

A light modulator supplied by Coherent Associates was on the components tray. The modulator uses the electro-optic effect in ADP (ammonium-dihydrogen phosphate crystal) to shift the phase of portions of a light beam passing through the modulator and change the intensity of the beam through interference effects. An identical modulator was stored in our laboratory. The modulator on the tray was mounted with an aluminum fixture that covered the apertures while the stored unit had plastic caps covering the apertures.

The modulator parameters measured were optical transmission, half-wave voltage, and roll-off frequency. Both the stored unit and the unit on the LDEF tray showed no changes in properties within experimental error upon remeasurement.

No measurable changes in optical transmission were found. The half-wave voltage and roll-off frequency were unchanged. These results are shown in Table 12.

TABLE 12.

ELECTRO-OPTIC MODULATOR CHARACTERISTICS

	Stored Device		Space-Exposed Device		
	Original	Remeasured	Pre-Launch	Post-Recovery	
Roll-Off Frequency	20 ±3	25 ±3	17 ±2	18 ±2	(Khz)
Half-Wave Voltage	240 ±14	250 ±15	227 ±3	225 ±5	(kV)
Optical Transmission	>98	>99	>98	>99	(%)

8.2 Channeltron (Microchannel) Plate

The two examples of this device were returned to the manufacturer and have since been lost. The manufacturer has looked for them, and agreed to complete remeasurement of these components if they can be found. It is assumed that they have been stored in a very safe place.

In the middle 1970's, devices of this type had potential application for optical computing. They were a possible means of transforming between coherent and incoherent radiation. Since that time, several other more promising technologies have been developed which show greater promise. From this perspective, microchannel plates no longer are as attractive for space system applications as they seemed twenty years ago. Therefore, we believe that the loss of these components is not critical.

8.3 Black Polyethelene

A few square inches of 1.5 mil thick black polyethelene (the type used for controlling weeds in gardens and controlling radiation in the laboratory) were attached to the tray after characterization in the extreme IR region. After recovery, the material was found to have been greatly changed in form. The thickness of the sheet was increased irregularly and the area was reduced. The distortion was such as to make it impractical to remeasure the material. Table 13 lists the prelaunch properties of the film. Clearly, this material was typical of other plastic materials carried aboard LDEF. In general, LDEF results as summarized in the NASA post-recovery symposia, have indicated that most plastics degrade in a low-orbit space environment[****] as a result of exposure to atomic oxygen.

TABLE 13.

EXTREME IR OPTICAL PROPERTIES
OF 1.5-MIL BLACK POLYETHELENE

Measured Thickness: 34 μm ±1 μm

λ (μm)	ν (cm^{-1})	n	k
294	34	1.53 ± 0.03	0.10
75.8	132	1.53	0.05
43.9	228	1.53	0.05

[****]Papers discussing the degradation of plastics in a space environment are reported in NASA Conference Publication 3134 as noted in Reference 15.

8.4 Holographic Crystals

Six holographic crystals were included in the component set. These were $LiNbO_3$ single crystals which contained holograms written shortly before the tray was assembled and stored at NASA Langely Research Center. This experiment was prepared by Drs. Russell Callen and Thomas Gaylord of the Georgia Tech School of Electrical Engineering.

The crystals were directly exposed to the space environment. Upon return, the crystals were inspected and found to be in good condition although fine indentations from micrometeroid impacts were observed on the exposed surface of each crystal. The holograms had disappeared during the years in storage and in space.

The crystals were in generally good condition. New holograms could be written and read, indicating that the functional aspects were unchanged.

Thermal cycling and age are considered to be the cause of the loss of the holograms.

IX. RADIATION SOURCES

9.1 Gas Lasers

HeNe and CO_2 gas lasers were included in the component set selected in the late 1970's. During the dozen years since that time, the applications for these lasers in space-based systems have largely been supplanted by semiconductor lasers which are better suited in several ways for many space system applications (small size, robust construction, low-voltage requirements). The potential degradation of other types of lasers similar to gas lasers such as eximer and dye lasers was expected to be comparable to the degradation of the HeNe and CO_2 gas lasers in the GTRI component set.

When the laser tubes were retested in May, 1990, no laser action could be obtained. The characteristics of the tubes suggested that the mixture of fill gas had changed during the period between initial and post-flight tests (about seven years). While the extended period in orbit was unplanned, this result is consistent with changes expected from gas diffusion through the glass envelope. The tubes were in otherwise good physical condition, having survived the launch and recovery phases without apparent degradation. The inability to achieve lasing action because of fill-gas composition changes was anticipated long before the recovery mission was launched. Gas lasers must be refilled every two years or so. For space-system applications, solid-state lasers should be used where possible.

9.2 Semiconductor Diode Lasers

The GaAlAs semiconductor diode lasers in the component set were of the single-heterostructure close-confinement structure which typified devices of this type manufactured in the early 1970's. Rapid progress has been taking place in laser diode technology over the past decades, and these diodes rapidly became obsolete as improved technology supplanted the 1970's fabrication techniques.

The diodes were tested using a silicon controlled rectifier circuit which provided low-voltage high-current pulses at a rate controlled by an external pulse generator. Diode radiation was monitored by a silicon photodiode instrument manufactured by UDT. Remeasurement indicated greater light output from all devices, a result believed caused by better collection efficiency of the post-recovery experimental arrangement rather than improved diode properties. Actual absolute diode power output is difficult to measure and was not attempted. The original equipment and geometry of the prelaunch measurements could not be duplicated. The performance of the diodes relative to one another had no significant change. As a result, we conclude that the space exposure and the years in storage did not degrade laser diode performance.

9.3 Light-Emitting Diodes

Two Monsanto MV10B GaAsP LED's were acquired for this set of components. The pair were marked with one and two stripes for identification. The voltage-current characteristic and the current-light output characteristic were measured. LED number one was stored. LED number two was placed on the LDEF tray and spent 69 months in space. Unit number two was mounted so as to have a direct view of the space environment through the aluminum sunshield which attenuated 55.2% of the incident radiation.

After flight, the LED's were examined. There were some marks on the flight unit indicating micrometeoroid impacts. These impacts were seen on top of the plastic dome, and around the edges of the dome. While the sunscreen provided some reduction in micrometeoroid particle flux, a surprising amount of particles passed through the screen and struck the tray surface and the mounted components. It should be noted that the direction normal to the sunscreen surface was 120° counterclockwise from the flight direction. Particles striking the tray surface were moving roughly normal to the flight direction, with some particles having a velocity component in the flight direction.

The original light collection system used for the GaAsP light-emitting diodes was duplicated for post-flight measurements. Therefore, pre-launch and post-flight data can be compared directly. The results are shown in Figure 33. As the figure shows, both the stored diode and the diode exposed to space reproduced their original characteristics quite well. It can be seen from the figure that the stored diode has somewhat greater light output for a given drive current, indicating greater quantum efficiency. At low currents, hysteresis occurs which makes exact reproducibility difficult.

The electrical and emission properties of the devices were essentially unchanged as a result of the passage of nearly thirteen years since their acquisition by GTRI including the nearly six years in space. The results indicate that the space environment, with its associated temperature cycling, ionizing radiation, and direct UV and solar radiation exposure, did not degrade the light emission properties of the LED's.

9.4 Nd:YAG Laser Rods

Because of their importance to electro-optic systems, Nd:YAG lasers were placed on the list of components to be included on the GTRI tray for the LDEF experiment. However, the size

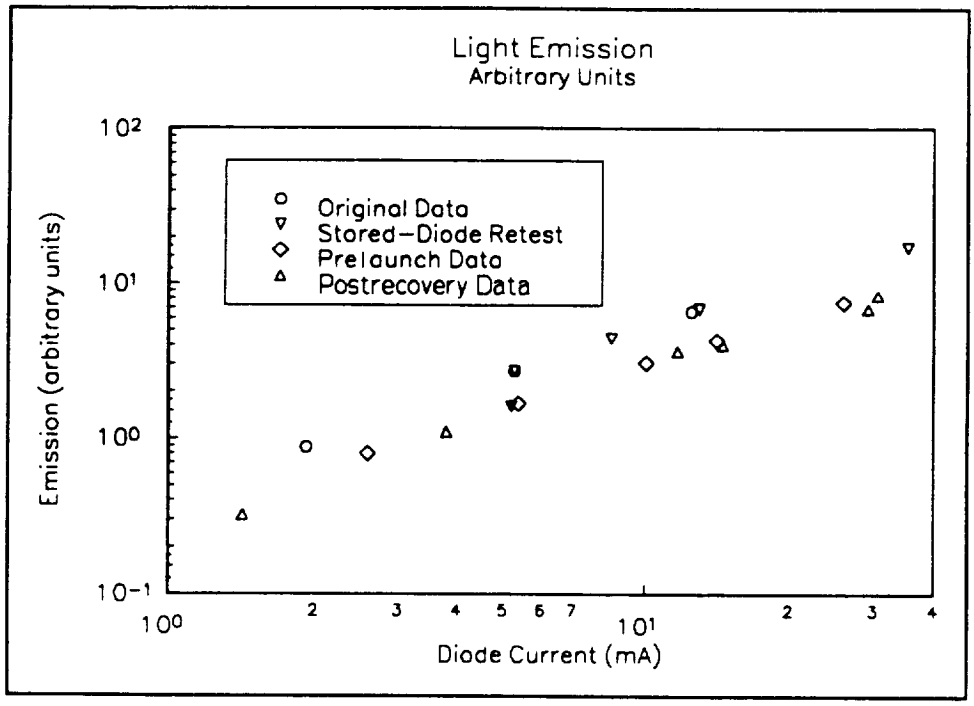

Figure 33. Light-emitting diode output vs drive current. Note that the control diode has slightly greater output than the flight unit.

and weight of a typical YAG laser suggested that only the items considered potentially sensitive to space exposure be included. Thus, the power supply, the optical bench and cavity, and the mirrors were not included. Only the Nd:YAG laser rods and an example of a flash lamp were placed on the tray. Potential degradation effects on laser mirrors were represented by a set of 25 multilayer-dielectric laser mirrors supplied by AFWC. Results for these mirrors are discussed in Section V.

Three Nd:YAG rods were measured before launch. Two were mounted on the tray beneath an aluminum cover (simulating the protection expected for a typical satellite installation) while the third was stored as a control. The rods were supplied by Litton/Airtron, and were measured using a YAG-laser system borrowed from the US Army, Redstone Arsenal. This system allowed the three rods to be mounted in series in the cavity such that any rod could be pumped at a variety of pulse rates.

During the thirteen years between prelaunch and postrecovery measurements, the laser cavity tarnished, and the entire laser needed refurbishment. The power supply was found to be unrepairable, and a substitute was used during the postrecovery measurements. Also, the pump lamps were replaced, as their output was below specifications. At the time of remeasurement, the YAG laser system was over twenty years old.

The measurements use the assumption that the relation between input pump energy and output laser-pulse energy is linear with an intercept on the pump-energy axis. The relation can be expressed as,

$$\text{Pump Energy (Joules)} = M \times \text{Pulse Energy (mJoules)} + C.$$

The constants M and C characterize a given rod in a given cavity. The constant, M, is known as the slope efficiency while C is the intercept. Because of the importance of the cavity in the measurements, it was considered important to use the same laser cavity for the remeasurement. In spite of these precautions, the renovation to the cavity made the cavity more efficient, and the remeasured coefficients outperformed the original measurements. The results of the measurements are listed in Table 13.

TABLE 14.

Nd:YAG-ROD PROPERTIES

	Control	Rod #1	Rod #2
Prelaunch			
Slope Efficiency, M (mJ/J)	24.6	22.6	23.6
Intercept, C (J)	7.6	7.1	7.0
Postrecovery			
Slope Efficiency, M (Mj/J)	36.2	35.0	35.2
Intercept, C (J)	3.8	3.1	3.1

The space-exposed rods and the control rod had the same relative change in measured characteristics. The relationship among the rods remains the same as in the original measurements. Our conclusion is that space exposure does not change the rod properties. Even the protected ¼λ coating on the ends of each rod survived in good condition.

9.5 Laser Flashlamp

A laser flashlamp for the tray and a second control lamp were supplied by ILC, San Diego, California. The lamps were characterized by the supplier both before launch and after recovery. The lamp was mounted under an aluminum cover to better simulate the minimum protection offered by a typical laser installation. The postrecovery characteristics of the flight lamp as well as those of the control lamp were found to be unchanged after exposure to the space environment. Results for measurement of the spectral emission of the ILS Type 1027B metal halide lamp mounted on the LDEF tray are shown in Figure 34. Similar lamps are used for laser rod pumping, and as position indicators for satellites.

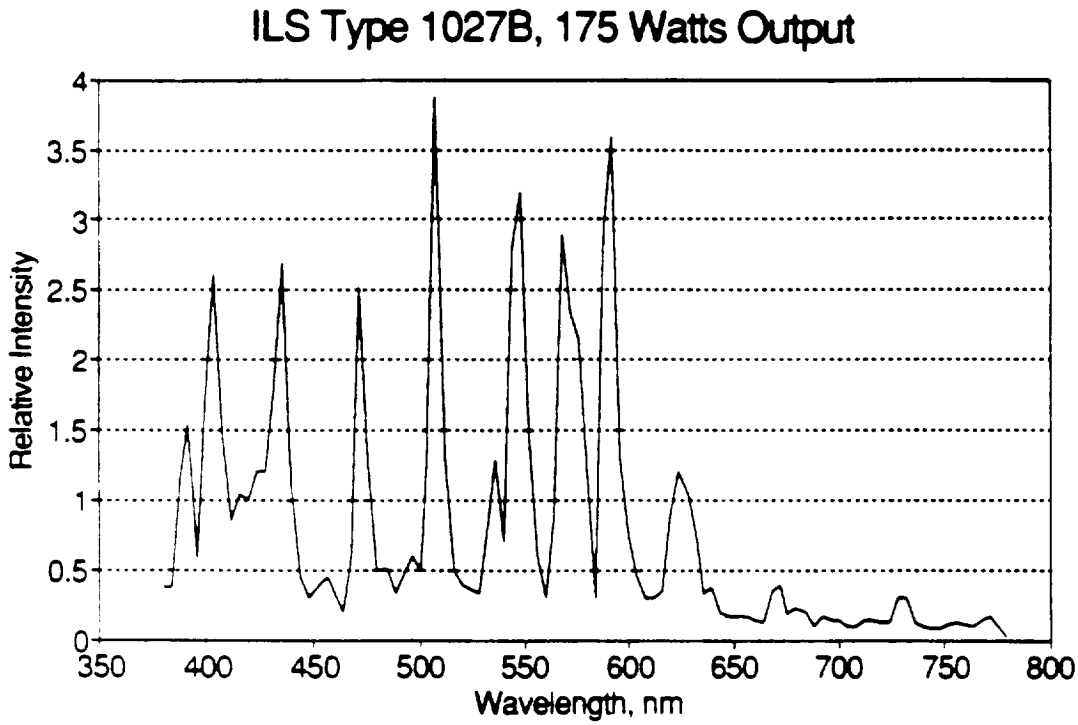

Figure 34. Spectral emission of the ILS type 1027B metal halide lamp mounted on the LDEF tray. Both the stored lamp and the space-exposed lamp had the same spectral output and did not change emission characteristics.

X. RADIATION DETECTORS

10.1 Silicon Detectors

Six large-area (800 mm^2) silicon detectors including two silicon gamma-ray detectors were located on a panel of the GTRI LDEF tray. These detectors consisted of a pair each of pn-junction diodes, pin-junction diodes, and pn-junction diodes mounted in a metal can (the gamma-ray detectors). The pn and pin devices were mounted so that they were exposed directly to the space environment.

Before-launch measurements included capacitance-voltage measurements and junction leakage measurements as well as sensitivity measurements. While expected applications of detectors in space would normally place them behind telescopes and away from direct viewing of the space environment, it was considered of interest to expose some detectors to space directly during the anticipated one year space exposure period for the possibility that something unanticipated might be found. The large-area silicon photodiodes were selected for this purpose.

The electrical measurements did not reveal any remarkable effects in any of these photodiodes as a result of almost 69 months in space. Only one detector, a pn-junction device, showed any increase in junction leakage, and the amount was less than 2 microamperes/cm^2 near depletion (although the leakage current almost tripled). The capacitance of the junctions was unchanged for all devices. Such effects are minor for the large-area devices used here. Figures 35 and 36 show leakage current for pn-junction devices 2 and 3, where device 3 is the detector that showed the increase in leakage. Device performance is not compromised by these effects.

The measured responsivity of the pn-junction detectors was near 0.44 A/Watt, in excellent agreement with the nominal value when manufactured. Current noise at 70 Hz and above was below 0.1 $Pa/Hz^{1/2}$, and well below the manufacturer's specification of 4 $Pa/Hz^{1/2}$.

Figure 37 shows results for a typical pre-launch and post-recovery capacitance measurement for a typical example from this set of detectors. All devices reproduced their prelaunch measurements. Figure 38 shows the noise measurements as a function of frequency for another example. Even with the usual 1/f noise at low frequency, the device noise remained low and well within the manufacturer's specification.

We have been unable to find any changes in the electro-optical properties of these large-area devices as a result of space exposure. However, the appearance of the diodes had changed somewhat.

An interesting feature of these detectors was the damage to the detector surface as a result of micrometeoroid impacts. There were from 0 to 2 impact craters on each of the large area detectors of such a size as to be visible to the unaided eye. A photograph of one such crater is shown in Figure 39.

The crater was found on the surface of pn-diode number 2. The I-V characteristics are shown in Fig. 35, and were not affected by the presence of the crater. The appearance of the crater indicates a diameter of 80- to 100-μm. The apparent direction of motion of the impinging particle is roughly aligned opposite to the velocity vector of the space vehicle as indicated by the arrow (ram direction). The velocity of the particle would be required to have a large component

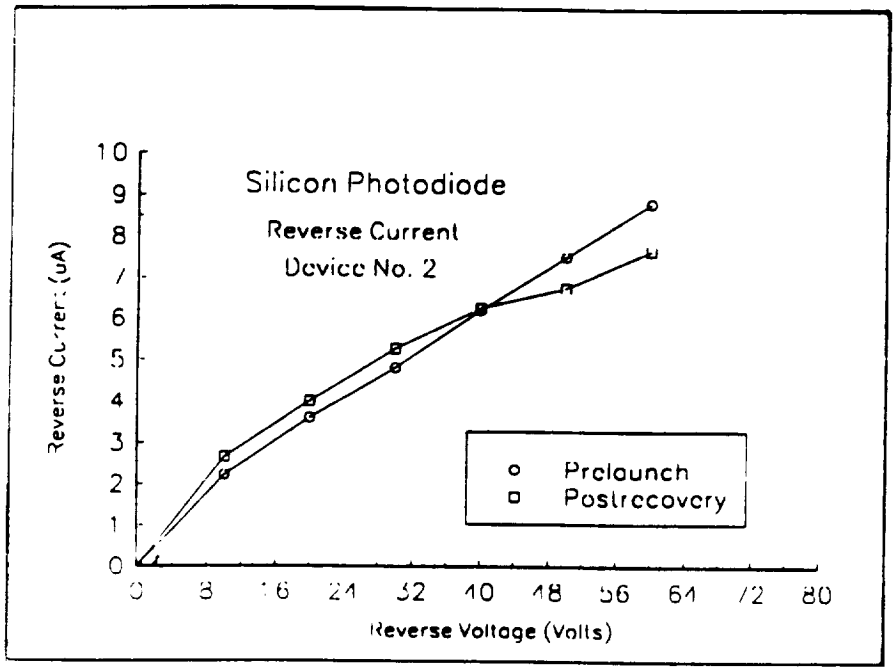

Figure 35. Leakage current for a large-area silicon diode (No. 2). The slight decrease in leakage current is not significant. The surface of this diode had a large (0.1 mm) impact crater (see Fig. 39).

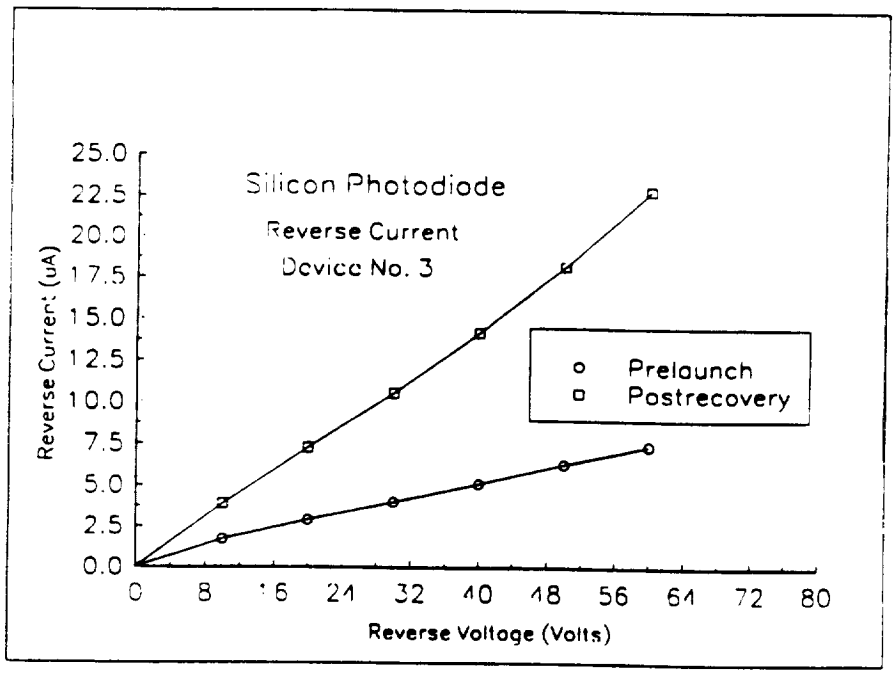

Figure 36. Leakage current for a large-area silicon (No. 3). For this diode, the leakage current increased.

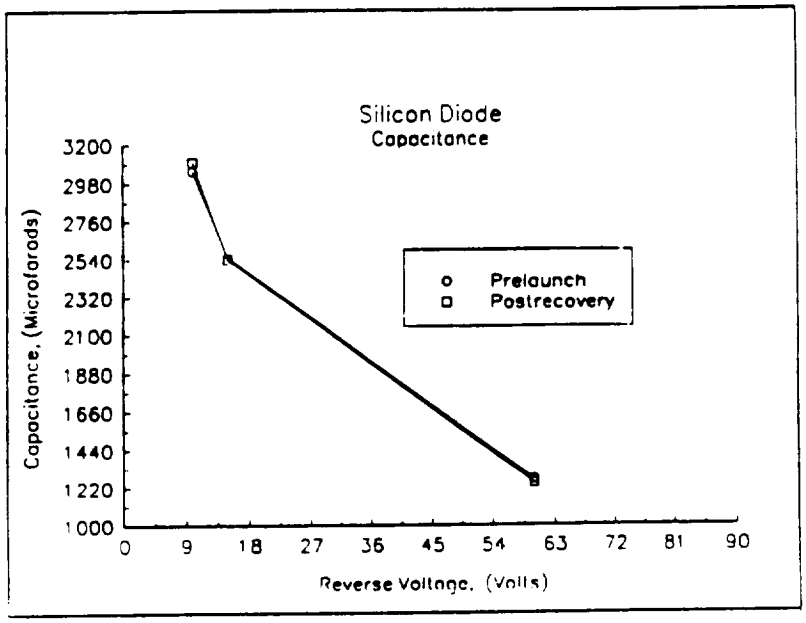

Figure 37. Prelaunch and Postrecovery capacitance measurements for a silicon pn-junction diode.

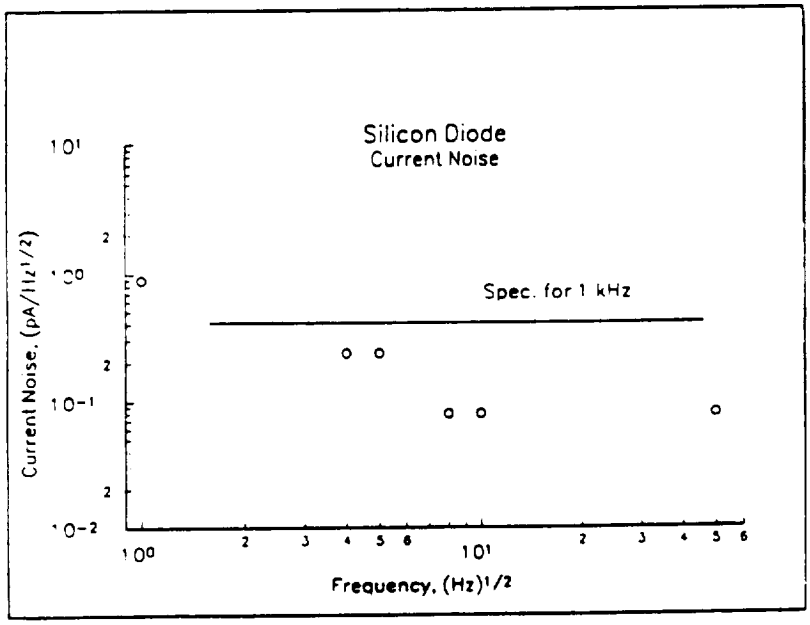

Figure 38. Noise Spectral Density for a silicon pn-junction diode. The noise is well within the manufacturers specification except in the Low-Frequency 1/f Region.

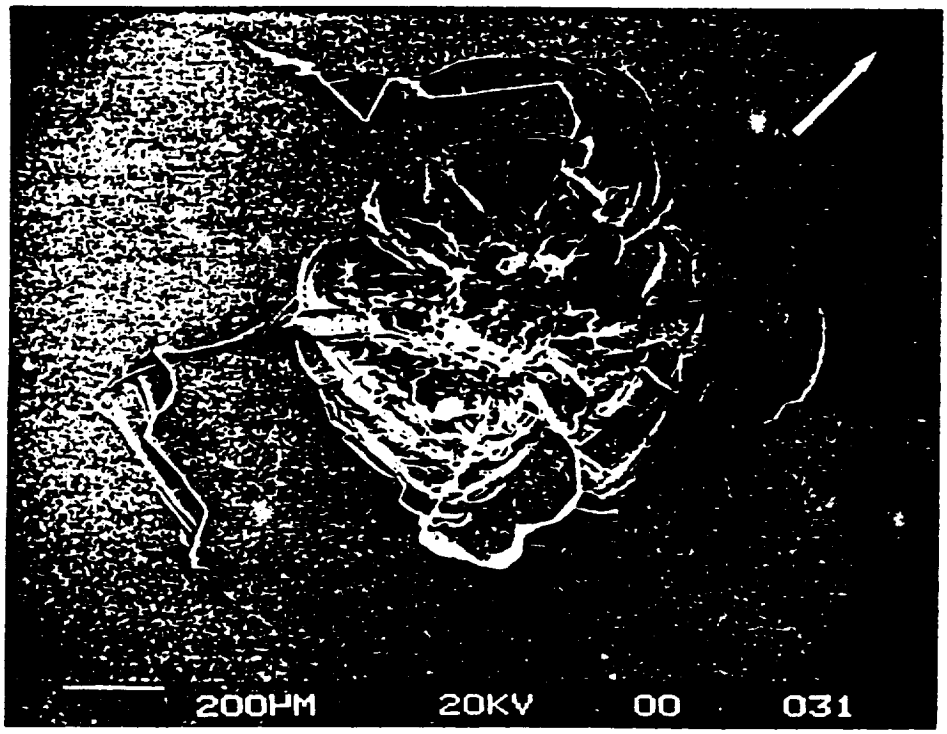

Figure 39 Scanning Electron Microscope photograph of an impact crater in a silicon pn-junction infrared detector. Note that the six-fold symmetry of the [111] face of the crystal is indicated by the direction of many of the cracks. The original photograph suggests that the passivation oxide may have cracked away from the substrate in some regions. No major changes occurred to the device properties.

normal to the detector surface as this surface is 120° behind the leading-edge surface. The remainder of the surface of this detector contained only very small craters that did not penetrate deeply into the silicon.

The silicon surface did not show as many small craters as the reverse side of the flat-pack chip carriers used to mount many of the other infrared detectors. These flat-pack carriers had a coating of gold on the reverse side (the side exposed to the space environment) which faithfully recorded many small particle impacts with crater diameters ranging from 10-μm to 100-μm.

Many of the infrared detectors in the component set were mounted in flat packs without windows. For these detectors, the flat packs (examined under an optical microscope) typically exhibited a darkened circular area where the back of the chip carrier was exposed directly to the space environment.

Microscope photographs show the darkening of the surface, sometimes edged with bright silvery material (presumably the Kovar material from the flat pack itself). The stained region is likely to be polymerized organic residue remaining on the surface. Post-recovery analysis of the LDEF has determined that such a polymerized surface coating will occur throughout the vehicle where organic residues are exposed to UV during the orbital period.

10.2 PdSi CCD Arrays

While the tray was opened for inspection in 1983, we took the opportunity to add two PdSi arrays to the collection of infrared detectors. These detector arrays were developed after the initial set of IR detectors was assembled. While these arrays must operate at temperatures near 77K, no cooling was provided for this experiment. The arrays use CCD's for array readout. CCD's are among the most sensitive semiconductor components to damage from ionizing radiation.

Two different chips were used. The first chip is a device containing process test devices. The second chip contained a Pd_2Si Schottky-barrier 32x63 IRCCD imaging array. The arrays were produced and characterized by the RCA Advanced Technology Laboratories which was disbanded as a result of the purchase of RCA by GE. The postrecovery characterization of the arrays was carried out by the David Sarnoff Research Center, and their data are analyzed in this section. The sample from the LDEF tray and a control sample (prepared from the same wafer as the spaceborne sample) were compared for shift of threshold bias voltage, dark current, and transfer inefficiency.

Radiation produces three different types of permanent degradation on CCD arrays. First, radiation effects can increase the thermal generation rate of minority carriers which increases the dark current and shortens the storage time of the device. Second, because of a tendency for some charge to be left behind in each transfer step from gate to gate, there is an inherent charge transfer loss in CCD's. This transfer loss or transfer inefficiency is enhanced by radiation and works to degrade image resolution. Finally, irradiation of a CCD causes a shift in the range of bias voltages in the propagation and transfer gates over which satisfactory operation can be obtained.

The major radiation damage mechanism in these devices is the production of positive charge which can be trapped in the SiO_2 insulator or at the semiconductor-insulator interface. The

amount of energy required to create a hole-electron pair in SiO_2 is 18 ev/pair. Thus, the dose must be adjusted to reflect the lack of pair production by lower energy radiation. However, because of the high energy of the electrons and protons incident on the LDEF, this correction is negligible. For 18 ev/pair, it can be calculated that 7.6 X 10^{12} pairs/cm^3 are created per rad(Si) dose.[32]

The devices were mounted on the tray so as to allow backside illumination. Ionizing radiation reached the arrays by passing through the holes in the sunscreen as well as by penetrating the solid aluminum portions of the screen. The total dose for these devices was calculated to be 68 krads(Si)/cm^2. As a result, the total density of hole-electron pairs created during space exposure would be 5.2 X 10^{17} pairs/cm^3. Of these, 95% would recombine quickly, and most of the defects produced by the remaining 5% would be expected to be removed by annealing. For an order of magnitude estimate, 5 X 10^{15} traps/cm^3 would be expected in the silicon dioxide gate insulators which could shift the bias potentials and provide traps the reduce the CCD transfer efficiency.

This estimated dose is about two orders of magnitude greater than the planned dose because of the extended time in orbit and a higher radiation flux than originally expected. A realistic space-borne sensor using an array of this type would mount the sensor in a cryogenic dewar at the focal plane of a telescope, and the assembly would likely be contained within additional structure providing additional radiation protection. Therefore, the results reported here represent manifestly worst case conditions.

Figures 37a and 37b show the construction and operation of the input and output stage of the serial output C-register of the array. The C-register was operated in a 2-phase clocking mode with a data rate near 2 X 10^5 to determine the effects of the space environment on transfer efficiency and operating voltages. The 2-phase mode provides better transfer efficiency than the usual 4-phase mode. A dc charge component could be added to the input charge at the input end of the C-register (fat-zero injection) as a means of improving charge transfer efficiency by filling fast trap states. Bias voltages were adjusted for maximum transfer efficiency.

The spaceborne array required a more positive bias (2.5V and 4.8V) than the control array. The cause of these shifts is not understood, and the direction of the shifts is opposite to the expected direction. Also, the magnitude of the shifts is greater than the threshold shifts measured in the test transistors included on the die. Transfer efficiencies exceeding 0.999 (or an inefficiency of 10^{-3}) will provide acceptable resolution. The control sample showed a transfer inefficiency of 10^{-4} at room temperature, and 2 X 10^{-3} a. 80K.

For the spaceborne sample, the transfer inefficiency at room temperature was 5 X 10^{-3}, and at 80K the inefficiency had degraded to 10^{-2}, indicating very poor operation. Injection of additional charge to fill the traps in the C-registers improves operation. With a charge injection equivalent to 2 X 10^6 electrons per pixel, the transfer efficiency at 80K improved to 0.998, equivalent to an inefficiency of 10^{-2}.

The density of ionizing-radiation-induced trap density can be estimated from the area of the CCD electrode (80-μm x 30 μm), the electrode thickness (1200 Å), and the calculated density of charge created by the ionizing radiation (5 x 10^{15} cm^{-3}). The product of these factors gives an estimated 1.5 x 10^6 traps per cm^3. This number is to be compared with the 2 X 10^6 electrons per pixel used as a fat zero charge injection to increase transfer efficiency. The agreement tends to

support the conclusion that the loss of transfer efficiency is the result of the rather excessive radiation dose received by the array while in orbit.

Dark current in the control and space-borne arrays was significant, equivalent to 1.3 X 10^6 and 2.5 X 10^6 electrons per pixel respectively at room temperature. At 80K, dark current drops by a factor of 5. The dark current in the control sample was very probably caused by defects in the B-register leaking into the C-register. The additional dark current in the spaceborne sample is believed to result from degradation caused by the ionizing radiation dose.

Threshold measurements for separate FET transistors on the chip provide an indication of process variations and the effects of space exposure. The measured values for threshold voltages for control and spaceborne devices are listed in Table 15. The threshold differences between control and spaceborne samples for the buried and surface channel devices were less than 0.5 V which would have a minimal effect on device operation. While some of this shift may be caused by radiation induced charging of the gate oxide, shifts of about half or less of this value would be expected from normal die-to-die process variations within a wafer. The test structures also allowed the potential difference between the buried channel potential minimum and the substrate to be measured. For the space-borne sample, the zero-bias values are very close to one of the reference samples, although this value also varies by about a volt between the reference samples.

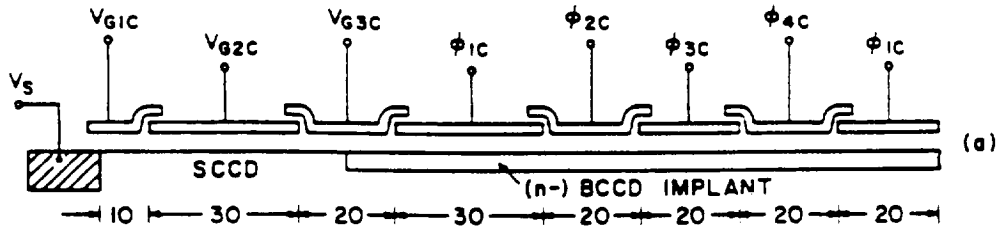

Figure 37a. Construction and operation of the input and output stage of the serial output C-register of the PdSi imaging array. The schematic of 15a shows the register layout.

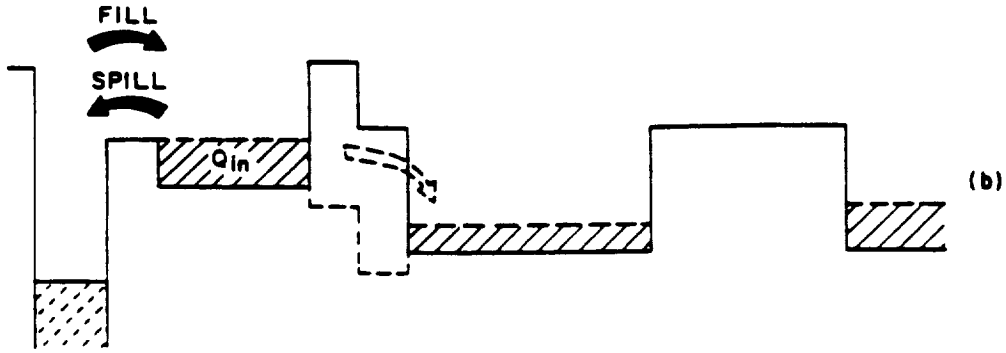

Figure 37b. Construction and operation of the input and output stage of the serial output C-register of the PdSi imaging array. This figure shows the charge flow during operation.

TABLE 15.

FET Threshold Voltages

Device Location	Control Sample Voltage	Spaceborne Sample Voltage
Surface Channel	-0.119 V	-0.214 V
Polysilicon 1 Buried Channel	-8.33 V	-7.92 V
Polysilicon 2 Buried Channel	-7.55 V	-7.11 V

The drain diffusion of the output transistor of the spaceborne array had a reverse=bias leakage current of about 10μA. While leakage current of this magnitude would have little effect on the amplifier operating point and transfer characteristics because the normal operating current is about 1 Ma, additional noise from this source could be important. There was no leakage current in other diffusion regions such as the C-register drain and test structures. Since the leakage current in this transistor is the exception, it may be caused by a defect and not related to the radiation dose.

In summary, several differences between control and spaceborne samples were observed. FET transistor threshold voltages exceeded normal process variations by a small amount, there was junction leakage in at least one case, the optimal CCD operating voltages changes, and CCD transfer efficiency degraded.

The changes in operating voltage are of a magnitude that can be accommodated by the drive electronics. As the parameters of the imaging system change, periodic calibration would allow for gradual changes in drive parameters.

The degradation in CCD transfer efficiency is the most serious issue to be addressed. A very large fat zero injection was necessary to provide minimal transfer inefficiency in the spaceborne device. The magnitude of the fat zero used in these measurements is in agreement with the estimated trap density and the resulting charge density arising from the received radiation dose.

The construction of these chips represents technology over ten years old. Since these arrays were produced, alternative insulating systems have been developed which provide greater radiation hardness. Newer devices also have shorter gate lengths and better transfer efficiency which suggests better performance in a radiation environment. Also, because of the known sensitivity of the arrays to radiation, radiation protection must be provided sufficient to limit the total dose to an acceptable level. Because of the protection provided by the metal cryogenic dewar and mounting structure, this requirement should pose no significant problem to the system designer.

10.3 InGaAsP Photodiodes

Measurements of four InGaAsP quaternary III-V detectors supplied by Rockwell Corporation indicate that these detectors also had no apparent degradation over a period of about ten years. These detectors were added to the component set in 1983 as substitutes for another type of detector which had become obsolete during the years following initial experiment tray assembly in 1979. The substitution was made during a final preparation period before delivery to NASA in 1983. The original data for the detectors did not accompany them, and were never sent to us.

However, the lack of initial data (now lost) is not crucial in this case. The pair of devices from the LDEF tray and the pair of devices stored in our laboratory have similar characteristics. The low junction leakage current for all four of these devices (5-Pa at 2 volts negative) indicates good temporal stability and a lack of any degradation caused by space exposure. These devices were mounted in flat packs, with the devices carried by the LDEF mounted upside down so that

the backs of the flat packs were exposed directly to the space environment. The detectors were returned to the Rockwell Science Center, where all the prelaunch and postrecovery measurements were performed. It should be noted that the leads to the diode contact pads eventually came off on all devices (both the stored and the space-exposed units) before and during shipment to the supplier for post-recovery measurements. These were experimental devices as supplied, and the technique for lead attach had not been optimized. Again, no space-related effects were observed.

10.4 Pyroelectric Detectors

10.4.1 Background

Pyroelectric detectors were considered an important type of radiation detector for space-based systems and were included in the LDEF electro-optic component set for several reasons. The reasons include their wide range of wavelength sensitivity from submillimeter wavelengths to ultraviolet (determined by the absorption of the coating applied to the surface of the pyroelectric material), and their ability to respond to infrared radiation without requiring cryogenic cooling. Sensitivities are not as high as for photoconductive and photovoltaic semiconductor detectors, but their convenience of application can make up for the difference in special applications.

Because of the potential NASA applications, a set of 29 pyroelectric detectors was assembled by Dr. James Robertson, NASA Langely Research Center, for the GTRI LDEF tray. GTRI provided an additional pair of detectors making a total of 31 devices in all. The detectors were calibrated by Dr. Robertson, and 10 were stored as controls. The other 21 detectors were placed on the tray for exposure to the space environment.

The 21 pyroelectric detectors mounted on the LDEF tray represented three different detector materials, three different window materials (as well as three with no window at all), and devices from several different manufacturers. The three types of pyroelectric material used in the detectors are Lithium Tantalate (LT or $LiTaO_3$), Strontium Barium Niobate (SBN or $Sr_{.66}Ba_{.33}Nb_2O_6$), and Triglycine Sulphate (TGS).

Signal and noise for the detectors were measured using a 500K black body with a selectable aperture, a preamplifier, and a Quan-Tech wave analyzer. Values of black-body detectivity (D^*) were typically in the mid 10^7 cm $Hz^{1/2}$ W^{-1} range. Measurements were made at different frequencies around 100 Hz.

Four detectors were mounted under an aluminum cover to reduce the ionizing radiation flux and eliminate the effects of ultraviolet radiation, while the remainder were mounted so as to expose them to the space environment. Detectors were cleaned with methyl alcohol before final assembly of the tray components, and were stored in a clean room both before assembly and after recovery. The assembled tray was stored at various locations for about six years before launch.

10.4.2 Experimental Details

Table 16 lists the pyroelectric detectors and indicates their window material if any, their location during the LDEF mission, and the change in signal, change in noise, and change in

detectivity as a result of over thirteen years of storage including (for 21 of the samples) nearly six years in space. Where more than one example of a specific detector configuration is listed in the table, the listed percent change represents the average for all examples of that configuration.

Figure 38 shows these results in pictorial form, with the height of the bars indicating the change in detectivity from the zero-change plane. The large reduction in D^* for the case of the TGS detector is the result of a large increase in detector noise. The signal for this detector was unchanged. The other TGS detectors with KRS-5 windows were not functional after recovery. No response to infrared radiation was found for either the TGS control detector and for the TGS detectors on the tray where KRS-5 windows were used.

An LT detector with a KRS-5 window also had a large drop in detectivity. As Table 16 indicates, for this detector the noise increased and the signal was reduced from the pre-launch measurements.

As indicated in the table, one LT detector had no signal after recovery. Two others were erratic in that measurements could sometimes be made, while at other times no signal could be obtained. Such behavior suggests that these detectors were manufactured with an unreliable fabrication technology, and intermittent open circuits were the source of the erratic behavior.

For the other detectors, the change in noise is within ±25 percent which is considered not to be significant. The change in signal for the other detectors is also small and not considered significant.

The three different window materials listed in Table 6 were removed from the detectors and examined at NASA Langely Research Center. For germanium (Ge) and Irtran II (zinc sulfide, ZnS) windows, there was no visible window damage or change in appearance. Also, the detectors using these windows suffered no significant loss in signal.

In contrast the KRS-5 (thallium-bromide-iodide, TlBrI) windows sustained noticeable damage during their exposure to the space environment. Postrecovery examination showed non-uniform cloudy (white) or slightly metallic-appearing regions on the front surfaces. Transmission losses through the windows were found to range from 17% to 50% with larger losses corresponding to regions with greater physical damage. No such changes were noted in transmission loss measurements in the infrared region through the window from a control detector. The lithium-tantalate infrared detector with the TlBrI window had a 38% drop in signal as indicated in Table 16. The signal loss is consistent with the transmission loss through the window.

After transmission measurements, the TlBrI windows were examined by electron microscopy. Surface analysis (to a depth of approximately 5 nm) indicated the presence of silicon (in the form of silicates) on the exposed windows with higher concentrations of Si in the regions of least damage and lower concentration in the regions of greatest damage. These measurements also indicted a change in the Tl:Br ratio at the space-exposed window surfaces. For the control window, the ratio was 1:1. For the space-exposed windows, the ratio was 4.6:1 in a low-damage region, became greater than 26:1 in regions of greater damage. Table 17 shows these results.

TABLE 16.

CHANGES IN PYROELECTRIC DETECTOR PERFORMANCE PARAMETERS

Detector Type	No. Of Samples	Window Material	Location During Experiment	% Change Signal	% Change Noise	% Change Detectivity
LT	1	none	control	-100	...this detector failed.	
LT	1	none	exposed	..this detector was erratic.		
LT	1	none	control	+2.5	-9	+6
LT	1	none	covered	+1.0	-10	+5
LT	3	none	exposed	-5.3	+1	-10
LT	2	Irtran II	control	-4.0	+23	-23
LT	1	Irtran II	covered	-3.5	+4	-6
LT	3	Irtran II	exposed	-6.7	+24	-25
LT	1	Irtran II	exposed	..this detector was erratic.		
LT	1	KRS-5	exposed	-38.0	+57	-61
LT	1	none	control	-14.0	-4	-3
LT	1	none	exposed	+7.0	+12	-2
SBN	1	Ge	control	+0.5	+1	0
SBN	1	Ge	covered	-1.4	+1	+2
SBN	4	Ge	exposed	-2.0	-22	+20
TGS	4	KRS-5	control	-100	No signal	
TGS	1	KRS-5	covered	-100	No signal	
TGS	2	KRS-5	exposed	-100	No signal	
TGS	1	Ge	exposed	0	+40	-30

Note: Irtran II is composed of ZnS.
KRS-5 is composed of TlBrI.

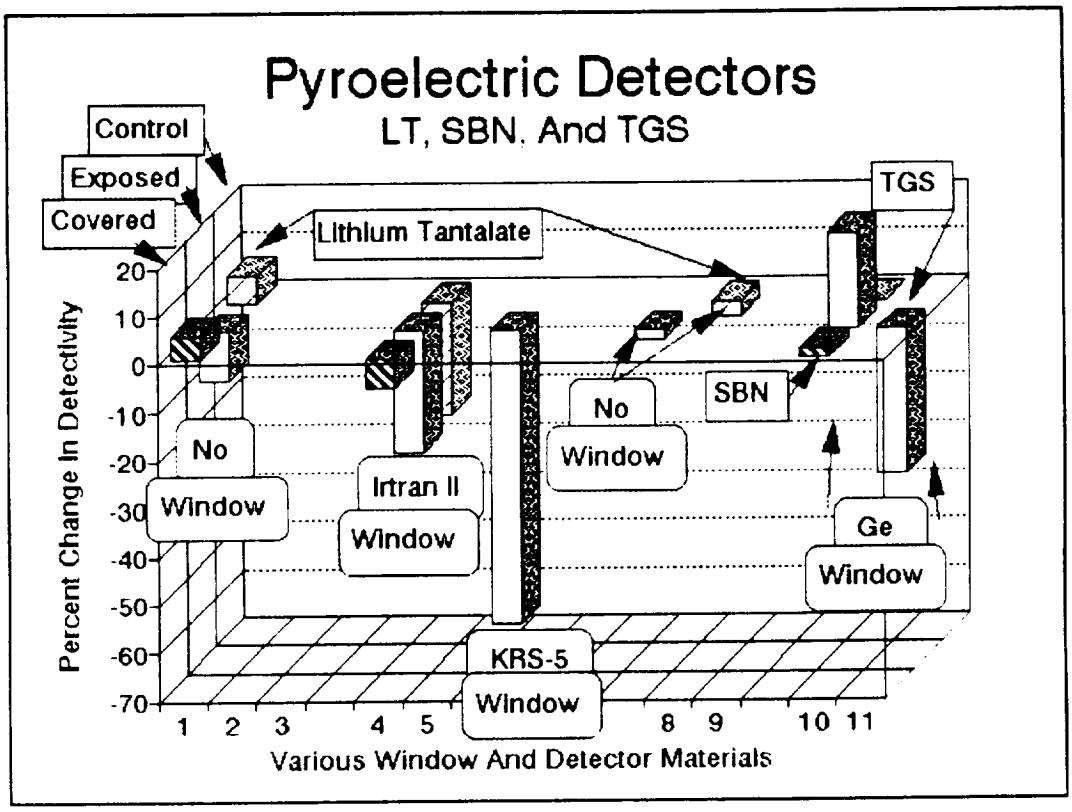

Figure 38. Change in detectivity for pyroelectric detectors.

TABLE 17.

MEASUREMENTS ON TlBrI (KRS-5) WINDOW MATERIALS

Window Condition	Si Concentration Atomic Percent	Tl:Br Ratio
Control (no exposure)	0	1:1
Space Exposed (Low Damage)	17	4.6:1
Space Exposed (High Damage)	6	>26:1

10.4.3 Conclusions

The results for this limited set of TGS pyroelectric detectors suggest that TGS detectors are unstable over the extended time period of this program. For the two other types of pyroelectric detector, the changes in performance over the approximately twelve year period are small, and there is no clear difference between the performance of the set of detectors on the LDEF tray after recovery and the control set after storage except for the lithium tantalate detector that failed and the two that were intermittent after recovery. The problem with these detectors may be caused by unreliable fabrication technology. The pyroelectric material does not degrade. For well-designed LT and SBN pyroelectric infrared detectors with stable window materials, reliable performance in space over time periods of a decade or more can be expected.

The measurements on the detector window materials indicate that there is a loss of bromine from the window material at the surface, and that the loss correlates inversely with the concentration of silicon on the surface. It is known from other LDEF measurements that silicon contamination was widespread on the surface of the satellite, and that metal halides exposed to the space environment do experience loss of the halide at the surface.[5]

Dr. Robertson speculates that the presence of the silicates and other contaminates (although non-uniform over the surface) tended to protect the windows from loss of bromine, and that it was this loss of the bromine component that caused the non-uniform damage to the KRS-5 windows. We have searched unsuccessfully for loss of the halide component in multilayer optical filters without success. The reason for the significant loss of bromine in these windows is not clear at this time, but are likely the result of solar radiation effects freeing weakly bonded halides.

10.5 Ultraviolet Light Detector

The ultraviolet radiation detectors listed in Table 1 were supplied by Dr. Gale Harvey of NASA Langley Research Center. Dr. Harvey also had a set of UV filters and windows as well as 35-mm film sensitive to the UV on the GTRI tray. These components represented NASA interest in UV component technology in the late 1970's.

At the time of this final report, measurement of the postrecovery detector performance has not been completed. Those readers interested in postrecovery UV detector properties are referred to Dr. Harvey for details.

10.6 PbS Detectors

A group of three PbS infrared detectors of size 2 X 2 mm, mounted in flat packs, optimized for operation at a temperature of 192K were measured and supplied to us in 1978. The detector size was 2x2-mm. An additional set of measurements was made in 1983 when the tray was opened for inspection and refurbishment. A final set of measurements was made in 1993. The PbS detector is known to have the potential for a temporal stability problem, controlled in this case by special processing during detector manufacture.[30] The radiation dose experienced by these detectors was estimated to be 600 rads (see Table 4, Section IV). The received dose is well below the level at which radiation effects would be observable. Damage thresholds in PbS detectors for neutrons are around the 10^{12} n/cm^2 level.[31] Furthermore, the degradation anneals logarithmically with time at room temperature. Damage acquired during the cold portion of the orbit would anneal during the warm portion, but the total received dose is well below the observable threshold.

Measurements for these detectors indicate that some changes in detector resistance, responsivity (signal output per unit signal input), and D^* (signal-to-noise) did occur over the fifteen year period since the original measurements, but the changes were not large. In general, the detectors survived storage and space exposure quite well. Table 17 lists values for detector resistance, responsivity, and detectivity for the three PbS detector modules. For module number 2, the 1983 data were unobtainable.

TABLE 17.

CHARACTERISTICS OF PHOTOCONDUCTIVE PbS DETECTORS
Detector Size: 2 X 2 mm. Chopping Frequency: ≈ 90 Hz

PbS 1 MΩ Load Resistor	Module Number 1			Module Number 2			Module Number 3		
	1978	1982	1993	1978	1983	1993	1973	1983	1993
Resistance, MΩ	3.5	2.6	2.1	0.9	-	1.5	1.6	1.4	1.6
Responsivity, (MV/Watt)	15.1	12.8	15.2	2.8	-	5.0	3.8	2.7	4.9
D^*, (10^{11}cm $Hz^{½}$/ Watt)	5.6	5.6	5.0	6.4	-	5.7	7.0	5.5	5.4

As this table indicates, small changes in detector properties occurred during room temperature storage during the 1978-1983 period. The drift in characteristics during this period is similar to the changes that occurred during the orbiting period. As a result, we conclude that such changes are to be expected, and periodic calibration of sensors using such detectors would be expected to be necessary. In addition to detector changes, potential changes in window and optics transmission as well as drifts in signal-processing electronics constitute other reasons to include calibration systems in space-borne sensors. The data also indicate that there is no intrinsic degradation mechanism in these detectors, and a long life, both in storage as well as in space, may be expected.

10.7 PbSe Detectors

A group of PbSe infrared detectors, mounted in flat packs, optimized for operation at a temperature of 192K were measured and supplied to us in 1978. The detector size was 4x4-mm. An additional set of measurements was made in 1983 when the tray was opened for inspection and refurbishment. The final set of measurements was completed in 1993. The PbSe detector is known to have a temporal stability problem, controlled by a special coating over the completed detector assembly to seal the polycrystaline detector material from atmospheric contamination.[32]

Again, radiation effects for these PbSe detectors (similar to the effects on PbS detectors) from radiation received while in orbit are well below the reported threshold for damage.[31] Table 18 lists values for detector resistance, responsivity, and detectivity for the three PbSe modules

TABLE 18.

CHARACTERISTICS OF PHOTOCONDUCTIVE PbSe DETECTORS
Detector Size: 4 X 4 mm. Chopping Frequency: ≈ 900 Hz

PbSe 1 MΩ Load Resistor	Module Number 1			Module Number 2			Module Number 3		
	1978	1982	1993	1978	1983	1994	1973	1983	1994
Resistance, MΩ	88	147	159	72	117	137	85	117	132
Responsivity, (kV/Watt)	6.4	8.9	6.7	5.15	10.7	6.2	7.5	9.4	10.1
D^*, (10^{11}cm $Hz^{½}$/ Watt)	1.1	1.6	1.2	1.1	0.93	0.77	0.97	1.1	1.1

A review of the data indicates that the detector resistance increased over the sixteen year period between initial and final measurements. The data also indicate that most of this increase took place during the first four years while the detectors were in storage before launch. After return from space, the additional increase was only about ten percent. However, the responsivity and sensitivity (D^*) values were fairly stable over this time period. The changes noted here would be considered significant for instruments designed to measure radiation values. However, an instrument designed for absolute radiation measurements would normally carry its own calibration system, and could accommodate the performance changes of the magnitude observed in this experiment.

In 1994, the lead-salt detectors used in this experiment (PbS and PbSe) are much less popular than in the 1960's and 1970's. They have been replaced by the cooled crystalline detectors based on InSb and HgCdTe materials which are usually assumed to be more stable and have no established intrinsic or temporal degradation modes.

In practice, the assumed stability has not always been found, and detector replacement is not uncommon. However, most of the problems are associated with HgCdTe detectors operated in the photoconductive mode where very high bias, typically several tens of milliamperes, can cause migration of contact metallization. Nonetheless, during the period of the LDEF program, the widespread use of PbS and PbSe infrared detectors has been in decline, and they are no longer available from the manufacturer of the detectors used in this program. They are still available from several sources including your local Radio Shack store.

10.8 InSb Detectors

A group of InSb infrared detectors, mounted in flat packs, was measured and supplied to us in 1978. An additional set of measurements was made in 1982 when the tray was opened for inspection and refurbishment. The final set of measurements was made in 1993. Santa Barbara Research Center (a part of the Hughes Corporation) supplied two linear detector arrays. The significant portions of these measurements are presented in Table 19.

While both photovoltaic and photoconductive InSb detectors have been manufactured, the photovoltaic configuration is by far the most common form and is the configuration of the detectors in this experiment. Reported measurements of neutron irradiation of InSb detectors indicated degraded performance.[33] The total dose required for observable degradation is far in excess of the dose received by these detectors while in orbit as calculated in Section IV, Table 4 of this report. No radiation effects were observed in the detector measurements reported here.

The numbering system for arrays had changed at the Santa Barbara Research Center during the years between 1982 and 1993, but is was possible to identify the original numbering scheme and correlate recent measurements with the original measurements. Some of the 20 detector elements in each array were of medium to poor quality, while others were excellent in terms of sensitivity and quantum efficiency (electron current per photon absorbed). It was found that the poorer quality detectors tended to behave in a less predictable manner. Detector arrays used in spacecraft will not make use of detectors that are not well behaved and near theoretical limits for sensitivity. The following discussion will be concerned with those detectors that were well behaved at the outset. Flooding InSb pv-detectors with light from fluorescent lamps affects the semiconductor surface so as to create an effective junction area larger than the actual junction area created during processing. As a result, the responsivity (current per photon) and the quantum efficiency are larger than expected. The collection area is undefined, and the detectors are not usable in this condition. When left in the dark, the detectors can typically recover their original characteristics. For the second of the two arrays reported here, the 1982 data indicated distortions suggesting that the array was flooded or flashed before measurement. These data were discarded, and only the 1978 and 1993 data are reported. For the these arrays, sensitivity (D^*) responsivity ($\Re$), and quantum efficiency (η) are reported.

For the first array, characteristics of good elements 4,5,6, and 7 are reported. The current at zero bias for the diodes is little changed from the original measurements (0.12-0.13 μA) under normal room light, while poorer quality diodes in the array tended to show higher current, indicating some degradation. The wire bonds on this detector array survived their storage and space exposure in good condition, and the detector properties retained their proper values.

TABLE 19

CHARACTERISTICS OF INSB DETECTOR ARRAYS

ARRAY NUMBER 1

D*, (10^{11} cm Hz/Watt)

Element Number	1	2	3	4
1978 Measurements	0.91	0.91	0.85	0.72
1982 Measurements	1.41	1.43	1.42	1.75
1993 Measurements	1.31	1.30	1.20	1.07

Responsivity ($\Re$, Amp/Watt)

Element Number	1	2	3	4
1978 Measurements	3.22	3.22	3.08	3.22
1982 Measurements	2.21	2.48	3.92	3.05
1993 Measurements	3.09	3.16	2.80	2.80

Quantum Efficiency, (η, percent)

Element Number	1	2	3	4
1978 Measurements	80	80	76	80
1982 Measurements	55	62	86	76
1993 Measurements	77	78	69	69

ARRAY NUMBER 2

D*, 10^{11} cm Hz/Watt)

Element Number	1	2	3	4	5	6	7
1978 Measurements	1.67	1.56	1.67	1.79	1.78	1.72	1.67
1993 Measurements	1.28	1.34	1.36	1.46	1.46	1.41	1.37

Responsivity ($\Re$, Amp/Watt)

Element Number	1	2	3	4	5	6	7
1978 Measurements	3.73	3.73	3.73	3.86	4.00	5.73	3.75
1993 Measurements	3.23	3.23	3.54	3.60	3.73	3.41	3.41

Quantum Efficiency, (η, percent)

Element Number	1	2	3	4	5	6	7
1978 Measurements	79	79	79	83	86	79	79
1993 Measurements	80	80	88	89	92	85	85

The second array had seven good detectors (1,2..,7) which were characterized for this experiment. No significant deterioration was noted in the current-voltage characteristics, and a slight increase in zero-bias current (0.14 μA to 0.17 μA) is not of real concern. Changes of this magnitude could be caused by small differences in received flux density as a result of a different cooled dewar surrounding the detector. Detector properties in this array are corrected for a 16% difference between the nominal detector area and the larger actual area.

Again, it should be stated that infrared detector manufacturing technology has improved during the fifteen years since these arrays were fabricated. Arrays with greater uniformity of detector properties are now available. While the stability of the good detectors in these arrays is satisfactory for space-based systems, changes in sensitivity of 30% are noted in the results listed in Table 19. Changes of this magnitude are found over periods of several years in detector arrays stored in laboratories or mounted as sensors in equipment of various types. If absolute calibration of received radiance is required of the sensors employing these detectors, some means for periodic recalibration of the sensor should be provided. Schemes for just such recalibration are a routine part of many contemporary sensors including space-based earth-observation satellites.

10.9 HgCdTe Detectors

10.9.1 Background

In Table 4, Section IV, the total radiation dose for detectors mounted in inverted flat packs was determined to be 600 rads or less. This is a modest radiation dose for HgCdTe (MCT) detectors. While both photovoltaic and photoconductive detectors suffer performance degradation in the presence of a radiation environment, photovoltaic devices begin to show degradation at around 10 Krad absorbed dose.[34] Photoconductive devices are even harder to radiation because of their small physical volume (thickness of 12-20 μm). Therefore, no radiation effects on the HgCdTe detectors were anticipated in this experiment, and none were seen.

Two manufacturers of HgCdTe infrared detectors supplied samples, mounted in flat packs, for the component set. Initial postretrieval measurements on photoconductive detectors indicated increased sensitivity. Results for the two sets of detectors are shown in Tables 20 and 21. Very likely, the increase in sensitivity shown in Table 20 was caused by a change in the field-of-view (FOV) for the detector. The sensitivity of the MCT detector is very dependent upon FOV. A reduction in the FOV decreases the photon flux on the detector which has the effect of increasing the photo-generated carrier lifetime (and decreasing photon-generated noise), and thus increases the photoresponse. The FOV and background flux for a detector-test station generally is not controlled carefully, and no records were ever available for this set of detectors.

10.9.2 Photoconductive MCT

A pair of photoconductive MCT detectors supplied by The New England Research Center (formerly Carson Alexiou then part of Magnavox, and, likely, be part of another company before this report is complete) were measured several times during the period covered by the LDEF

program. Table 20 summarizes the results. As mentioned on the preceding page, the apparent improvement in sensitivity of this detector is believed to be the result of use of newer test stations with reduced background flux and, therefore, lower background noise.

TABLE 20.

CHARACTERISTICS OF HgCdTe PHOTOCONDUCTIVE DETECTORS

All Measurements At A Chopping Frequency Of 1 kHz

Date of Measurement	Det. #	R_o Ω	Noise V μV/√Hz
11/11/78	1	38.0	3.7
	2	53.5	22.5
11/18/82	1	38.3	1.0
	2	53.6	4.2
10/12/92	1	69.4	2.2
	2	90.0	3.2

Date of Measurement	Det. # @ 1 Khz	D^*_{BB} 10^9	D^*_λ in 10^9	λ_p/λ_{co} in 10^9
11/11/78	1	3.85	11.8	10.6/13.7
	2	3.26	9.4	10.0/12.0
11/18/82	1	6.6	20.2	-
	2	4.5	12.9	-
10/12/92	1	12.8	37.8	- /14.0
	2	14.0	37.4	- /11.9

TABLE 21.

CHARACTERISTICS OF HgCdTe PHOTOCONDUCTIVE DETECTOR ARRAYS

MEASUREMENTS OF PEAK DETECTIVIY, $D^*(\lambda_p)$

All Units In This Table Are In 10^{11} cm Hz½ / Watt
These Detectors Are Manufactured For The 3 μ - 5 μm Waveband

Array Number 1

Element No. Date of Measurement	1	4	6
1978	3.8	4.3	3.1
1993	3.8	4.3	2.9

Array Number 2

Element No. Date of Measurement	1	2	4	5	6	7
1978	5.4	5.5	4.6	3.9	3.9	3.4
1993	5.3	4.4	4.2	4.2	4.3	4.2

Array Number 3

Element No. Date of Measurement	1	2	3	4	6	7
1978	4.3	4.0	4.3	4.0	4.1	3.9
1993	3.2	3.7	3.6	3.9	3.9	3.6

The measurements reported in Table 21 show quite good agreement between the 1978 measurements and the 1993 measurements of detectivity. While some of the detectors were a bit larger than the nominal size of 0.002-inches square, the small error incurred will be the same for both the earlier and later sets of measurements. A correction would raise the measured sensitivity of the detectors by about 20%.

The good agreement may be the successful result of a serious attempt to reproduce the original background conditions of the original set of measurements. This is quite difficult to do, and the background radiation for the earlier and later measurements will certainly not be identical. However, it is believed that the difference is not large. The good agreement between the two data sets for three arrays indicates quite strikingly that long-term storage followed by several years of exposure to low-earth-orbit conditions does not degrade these MCT photoconductive detectors.

10.9.3 Photovoltaic MCT

Photovoltaic detectors using HgCdTe were also retested and found to be comparable in their characteristics to the original measurements. Results for two linear arrays from the LDEF and one control array are presented. The results are presented in Table 22. For the original measurements, amplifiers with feedback resistors of 10, 20, and 66 MΩ were used. The retest used an amplifier with a 20 MΩ resistor only.

Some deterioration was found for some elements in these photovoltaic detector arrays. For the control array, the wire connections to the detector bond-pads were made using a silver-filled epoxy. For the two other arrays, the wires were welded to the pads (the more conventional approach). Some elements were open circuit (not connected) because the metallization on the semiconductor surface had peeled away. Yet, other detector elements which did not exhibit such metallization peeling were also open circuited. Some corrosion or other deterioration mechanism in the silver-filled epoxy may have caused problems with this earth-bound control array. Two of the elements had deteriorated somewhat, while the other two still retained their sensitivity.

In array number 1, the sensitivity of the detector elements was little changed from the original values, but array number 2 showed deterioration for elements 3, 9 and 11. Element number 4 has increased in sensitivity. The others show little change.

Our conclusions for these HgCdTe PV arrays are that fabrication technology in the mid-1970's was the cause of at least some of the observed deterioration, but that the intrinsic characteristics of the detector elements need not degrade. The fact that many of these elements have not lost their original sensitivity indicates that the intrinsic detection mechanism is stable with time, and that the temperature cycling and other effects of low-earth orbit are not a source of problems for detector operation. However, the space-exposure effects may result in problems with electrical contacts or other mechanical or fabrication related difficulties which affect array performance.

TABLE 22.

CHARACTERISTICS OF HgCdTe PHOTOVOLTAIC INFRARED DETECTORS

PV MCT Array #1 Element Number	1	2	3	5	6
1983 Measurement D^* (10^{11} cm $Hz^{1/2}$/Watt)	1.8	2.2	2.4	1.8	2.2
1993 Measurement D^* (10^{11} cm $Hz^{1/2}$/Watt)	1.8	1.8	2.0	1.8	1.6

PV MCT Array #2 Element Number	1	3	4	8	9	10	11
1978 Measurement D^* (10^{11} cm $Hz^{1/2}$/Watt)	1.9	1.0	0.69	1.4	1.4	open	1.3
1993 Measurement D^* (10^{11} cm $Hz^{1/2}$/Watt)	1.2	0.3	1.24	1.1	0.7	0.3	0.9

PV MCT Control Array Element Number	1	3	10	13
1978 Measurement D^* (10^{11} cm $Hz^{1/2}$/Watt)	2.1	1.8	2.9	2.1
1993 Measurement D^* (10^{11} cm $Hz^{1/2}$/Watt)	1.8	1.1	2.2	0.55

XI. SUMMARY AND CONCLUSIONS

In this report, we have emphasized the components that were affected by the space environment. However, most components were unchanged. Most hard, metallic, ceramic, and covalently-bonded materials are not degraded by space exposure. Laser rods, modulators, and infrared detectors are examples. The organic pyroelectric radiation detector, TGS, did degrade. Other organic materials such as black paints and the polyethylene sheet degraded. This multilayer films also degraded. As mentioned in this report, newer technology may eliminate this problem.

Construction can also play an important role in degradation. For example, interfaces such as the SiO_2-Si interface in CCD's or the interface between deposited layers in multilayer filters and mirrors has been found to be a source of component degradation in the work described in this report and in the cited references. Degradation in LEO is difficult to reduce to one or two rules. Summaries in several sections of this report provide insight into degradation mechanisms.

The conclusion to this study should be that degradation in many components is difficult to anticipate or predict. System designers should be aware of the results of this and other similar experiments as reported in the literature and in NASA reports. To oversimplify the results but leave a simple slogan that can be remembered, we suggest the following:

Hard and simple things are stable; soft and complex things degrade.

XII. ACKNOWLEDGEMENTS

Many colleagues and students contributed to this program over its decade-long existence at the Georgia Tech Research Institute. Prominent among the group were R. G. Shackelford, J. J. Gallagher, D. O. Gallentine, Marie Fair, Kevin Bottler, Dr. C. W. Gorton, Dr. Garth Freeman, and Dr. Amitava Roy. The assistance of these and many other contributors is acknowledged and appreciated. The assistance and support of personnel at the NASA Langely Research Center has been of great value to this program from the outset. In particular, help from the experiments managers including John DiBattista, Lenwood Clark, and James Jones, and the LDEF Chief Scientist, William H. Kinard, helped smooth out many difficult periods. The program has been supported by the Langely Research Center, Hampton, Virginia.

Suppliers of components for this LDEF tray included the NASA Langely Research Center, New England Research Center, Santa Barbara Research Center (Dr. Peter Bratt), Corion, Coherent Associates, Coherent Radiation, Galileo Electro-Optics, Night Vision And Electro-Optic Center, Air Force Weapons Laboratory, RCA Corp.(John Tower), ILC Technology, Lockheed Missiles & Space Corp., Litton/Airtron, Quantrad Corp., Eastman Kodak, and the Rockwell Science Center.

XII REFERENCES

1. E. V. Benton, W. Heinrich, T. A. Parnell, T. W. Armstrong, J. H. Derrickson, G. T.Fishman, A. L. Frank, F. W. Watts, Jr., and B. Weigel, "Ionizing radiation exposure of LDEF (Postrecovery estimates)," Nuclear Tracks and Radiation, 20, 75-100 (1992).

2. Roger J. Burassa and James R. Gillis, "LDEF Atomic Oxygen And Fluence Calculations," Boeing Defense and Space Group, January 18 (1991).

2. Roger J. Burassa and James R. Gillis, "LDEF Atomic Oxygen And Fluence Calculations," Report, Boeing Defense and Space Group, January 18 (1991).

3. William M. Berrios and Thomas R. Sampair, "Long Duration Exposure Facility, Post-Flight Thermal Analysis," NASA TM-104208 (1992).

4. Keith Havey, Arthur Mustico, and John Vallimont, "Effects Of Long-Term Environment Exposure On Optical Substrates And Coatings," presented at the Second LDEF Post-Retrieval Symposium, San Diego, California, June 1-5 (1992).

5. Gale A. Harvey, "Effects Of Long-Duration Exposure On Optical System Components," LDEF-69 Months In Space, NASA Conf. Pub. 3134, 179-196 and 1327-1340 (1992).

6. Keith Havey, Arthur Mustico, and John Vallimont, "Effects Of Long-Duration Space Environment Exposure On Optical Substrates And Coatings," presented at the Second LDEF Post-Retrieval Symposium, San Diego, California, June 1-5 (1992).

7. M. D. Blue and D. W. Roberts, "Effects Of Space Exposure On Optical Filters," Appl. Opt., 31, No. 20, pp. 5299-5304 (1992).

8. Fred Goldstein, "Optical Filters," in Methods Of Experimental Physics, Daniel Malacara, ed., Vol. 25, Academic Press, Inc. (1988), pp. 273-301.

9. C. A. Nicoletta and A. G. Eubanks, "Effect of Simulated Radiation on Selected Optical Materials," Appl. Opt., 6, pp. 1365-1370 (1972).

10. M .T. Shetter and V. J. Abreu, "Radiation Effects On The Transmission Of Various Optical Glasses And Epoxies," Appl.Opt. 18, pp. 1132-1133 (1979).

11. S. F. Pellicory, E. E. Russell, and L. A. Watts, Radiation Induced Transmission Loss In Optical Materials," Appl. Opt. 18, pp. 2618-2621 (1979).

12. P. N. Grillot and W. J. Rosenberg, "Proton Radiation Damage In Optical Filter Glass," Appl. Opt. 28, pp. 4473-4477 (1989).

13. Optical Design, U.S. Government Publication, MIL-HDBK-141, Military Standardization Series (5 October 1962), Paragraph 20.4.8.2.2.

14. J. S. Seeley, R. Hunneman, and G. J. Hawkens, "Exposure To Space Radiation Of High-Performance Infrared Multilayer Films And Materials Technology Experiment (A0056)," Final Report, Reading University, April (1991).

15. These observations were reported by several investigators in Environmental Effects-Materials, Part 2, LDEF-69 Months In Space, NASA Conf. Pub. 3134, Edited by Arlene S. Levine (In Three Volumes, 1992).

16. Erik J. Linden, "Aerospace Electronic Materials: Applications/Environments/Effects," Electro-Technology, December, 125-131, 68 (1961), and references therein.

17. T. M. Donovan, J. M. Bennett, R. Z. Dalbey, D. K. Burge, and S. Gyetvay, "Space Environmental Effects On Coated Optics," LDEF-69 Months In Space (Proceedings of a symposium sponsored by the National Aeronautics And Space Administration and held in Kissimmee, Florida), NASA Conf. Pub. 3134, pp. 1361-1375 (1992).

18. Optical Design, U. S. Government Publication MIL-HDBK-141, Military Standardization Series (5 October 1962), Paragraph 20.10.5.1.

19. Cryolite is a sodium-aluminum fluoride compound. See "The Infrared Handbook," William L. Wolfe and George J. Zissis, Eds., Environmental Institute of Michigan (1978).

20. J. R. Grammer. W. H. Alff, M. D. Blue, and S. Perkowitz, "Far-Infrared Reflectance Of Optical Baffle Coating Materials," in Thermophysics and Thermal Control, Vol. 66 of Progress in Astronautics and Aeronautics, New York, pp. 39-46 (1978).

21. W. H. Alff, M. D. Blue, and S. Perkowitz, "Reflectivity Of Radiation Absorbing Coatings," in ***Proceedings of the Third International Conference of Submillimeter Waves and Their Applications*** (The Physical Society, Univ. of Surrey, Guildford, U. K., pp. 276-277 (1978).

22. D. W. Bergener, S. M. Pompea, D. F. Shepard, and R. P. Breault, "Stray Light Rejection Performance Of SIRTF: A Comparison," Proc. SPIE Int. Soc. Opt. Eng. (USA) 511, pp. 65-72 (1984).

25. D. B. Betts, F. J. J. Clarke, L. J. Cox, and J. A. Larkin, "Infrared Reflection Properties Of Five Types Of Black Coatings For Radiometric Detectors," J. Phys. E (GB) 18, pp. 689-696 (1985).

22. S. Ungar, J. Mangin, M. Lutz, G. Jeandel, and B. Wyncke, "Infrared Black Paints For Room And Cryogenic Temperatures," Proc. SPIE Int. Soc. Opt. Engr. (USA) 1157, pp. 369-376 (1989).

25. S. M. Smith, "Specular reflectance of optical black coatings in the far infrared," Appl. Opt. 23, 2311-2326 (1984).

26. S. M. Smith, "The specular reflectance of IR-opaque coatings," Int. J. Infrared Millimeter Waves 5, 1589-1595 (1984).

27. M. D. Blue and S. Perkowitz, "Reflectivity of common materials in the submillimeter region," IEEE Trans. Microwave Theory Tech. MTT-25, 491-493 (1977).

28. S. M. Smith, "Specular reflectance of optical-black coatings on the far infrared," Appl. Opt. 23, 2311-2326 (1984).

29. J. R. Duffey, W. W. Powell, S. H. Song, D. G. Manpearl, and A. H. Kalma, "Gamma Radiation Tests Of Bulk And IBC Si:As Mosaic Detector Arrays," Proc. IRIS Detector, Vol. II, 147-162 (1986).

30. W. L. Eisenman, "Properties of photoconductors," AEC Accession Number 2342, Report Number AD631225, (1964).

31. Norman J. Rudie, Principals & Techniques of Radiation Hardening, Western Periodicals Co., N. Hollywood, CA,91603, Vol. II, 17-21 (1976).

32. K. S. Pilger, "Storage and aging data on PbSe infrared detectors." NASA Accession Number N66-28640, Report Number AD631225, (1966).

33. N. D. Wilsey, C. S. Guenzer, B. Molnar, and W. J. Moore, "A Comparison of Fast Neutron Effects in Photoconductive and Photovoltaic InSb Infrared Detectors," IEEE Trans. Nucl. Sci., NS-22, 2448-2455 (1975).

34. G. M. Williams, R. E. DeWames, A. H. B. Vanderwyck, and E. R. Blazejewski, "Radiation Response of HgCdTe Photodiodes," Proc. IRIS Detector, Vol. II, 57-68 (1988).

REPORT DOCUMENTATION PAGE

Form Approved
OMB No. 0704-0188

1. AGENCY USE ONLY (Leave blank)	2. REPORT DATE	3. REPORT TYPE AND DATES COVERED
	October 1994	Contractor Report

4. TITLE AND SUBTITLE
Investigation of the Effects of Long Duration Space Exposure on Active Optical System Components

5. FUNDING NUMBERS
C NAS1-14654
WU 506-43-61-07

6. AUTHOR(S)
M. D. Blue

7. PERFORMING ORGANIZATION NAME(S) AND ADDRESS(ES)
Georgia Institute of Technology
Georgia Tech Research Institute
Atlanta, GA 30332

8. PERFORMING ORGANIZATION REPORT NUMBER

9. SPONSORING/MONITORING AGENCY NAME(S) AND ADDRESS(ES)
National Aeronautics and Space Administration
Langley Research Center
Hampton, VA 23681-0001

10. SPONSORING/MONITORING AGENCY REPORT NUMBER
NASA CR-4632

11. SUPPLEMENTARY NOTES
Langley Technical Monitor: James L. Jones
Final Report

12a. DISTRIBUTION/AVAILABILITY STATEMENT
Unclassified--Unlimited

Subject Category 74

12b. DISTRIBUTION CODE

13. ABSTRACT (Maximum 200 words)

This experiment was exposed to the space environment for 6 years on the Long Duration Exposure Facility (LDEF). It investigated quantitatively the effects of the long-duration space exposure on the relevant performance parameters of a representative set of electro-optic system components, including lasers, radiation detectors, filters, modulators, windows, and other related components. It evaluated the results and implications of the measurements indicating real or suspected degradation mechanisms. This information will be used to establish guidelines for the selection and use of components for space-based, electro-optic systems.

14. SUBJECT TERMS
Electro-optics; Space environmental effects; Long Duration Space Exposure

15. NUMBER OF PAGES
92

16. PRICE CODE
A05

17. SECURITY CLASSIFICATION OF REPORT	18. SECURITY CLASSIFICATION OF THIS PAGE	19. SECURITY CLASSIFICATION OF ABSTRACT	20. LIMITATION OF ABSTRACT
Unclassified	Unclassified		